UNIVERSITÀ DEGLI STUDI DI PADOVA

Dipartimento di Fisica e Astronomia "Galileo Galilei"

Corso di Laurea Magistrale in Fisica

Tesi di Laurea

Unmagnetized Atmospheres around Neutron Stars

Relatore

Prof. Roberto Turolla

Correlatore

Dr. Roberto Taverna

Laureando

Edoardo Zatti

Anno Accademico 2017/2018

Abstract

Compact objects, black holes, white dwarfs and neutron stars, are the endpoints of the evolution of stars with different initial masses. The existence of stars made essentially of neutrons was first hypothesized in the 1930's when it was realized that gravitational contraction could be balanced by the pressure of degenerate fermions obeying the Pauli principle. Neutron stars, with mass of 1-2 solar masses and radius of 10-20 km, are the densest known objects in the present universe. They were no more than a theoretical curiosity until 1967, when Hewish and Bell discovered the first radiopulsar. Since then our understanding of neutron stars and of their observational manifestations moved steadily on. However, many key questions in neutron star astrophysics are still unanswered. In this work I study the reprocessing of thermal radiation by an atmosphere which surrounds the star and which is key in shaping the emergent spectrum. This bears directly to the measure of fundamental neutron star properties. Goal of the thesis is to review the radiative transfer in a medium and apply it to model neutron star atmospheres in both radiative and hydrostatic equilibrium.

Contents

List of Figures

Introduction

Neutron Stars (NSs) are the most compact objects in the universe endowed with a surface. They represent an ideal laboratory to understand the physics in extreme condition, which can not be reproduced. NSs are born very hot and then progressively cool down emitting neutrinos and thermal radiation. For some 10^5 yr their surface temperature is about a million K and they shine as soft X-ray sources. Observations of their surface emission are key, since they provide direct information on the physical conditions of the star surface layers (effective temperature, chemical composition and surface gravity) and, even more important, they allow for a direct measurement of the star radius. A physically model for the surface emission is key in order to correctly interpret X-ray data. In the past it was assumed that the star surface emits blackbody radiation. However, starting from the late 1980's, the role of a thin gaseous atmosphere in reprocessing the outgoing radiation was realized. This work focuses on unmagnetized atmosphere models with the aim of computing the emergent spectrum. The role of different chemical compositions, from hydrogen to heavy elements, is examined, together with the effects produced on the spectrum by different stellar parameters. The resulting spectra are compared with the blackbody distribution, with particular attention on the different behaviour between that a light-element atmosphere can produce with respect to an heavy-element one.

The method used to solve the radiative transfer is based on an iterative scheme starting from an approximated temperature profile. The procedure is divided into two parts: in the first one the calculation of the atmospheric structure is performed while in the second one the radiative transfer is computed using the Schwarzschild-Milne relation. To complete an iteration, a correction of the temperature through the Lucy-Unsöld formula is applied. A new iteration starts computing the structure and the flux again until the

correction is minimal. The implementation of the model has been written in Fortran 95.

Chapter 1

Neutron Stars

Neutron Stars are the most compact objects known in the universe and matter can reach supra-nuclear densities in their interior. They have typical masses $M \sim M_\odot$ and radii $R \sim 10\,\mathrm{km}$. Neutron stars have a strong surface gravity $g \sim GM/R^2 \sim 2 \times 10^{14}\,\mathrm{cm\,s^{-2}}$ and their average mass density is $\bar{\rho} = 3M/(4\pi R^3) \sim 7 \times 10^{14}\,\mathrm{g\,cm^{-3}} \sim (2{-}3)\rho_0$ where $\rho_0 \sim 2.8 \times 10^{14}\,\mathrm{g\,cm^{-3}}$, the *normal nuclear density*, is the mass density of nucleons in heavy atomic nuclei. They are endowed with strong magnetic fields which usually range between $10^8{-}10^{15}\,\mathrm{G}$ and their rotational period varies from 10^{-3} to $10\,\mathrm{s}$. The theoretical prediction of the existence of NSs was made in 1934 by W. Baade and F. Zwicky (see Baade & Zwicky, 1934) who analyzed the observations of supernova explosions. They hypothesized that *"supernovae represent the transitions from ordinary stars to neutron stars, which in their final stages consist of extremely closely packed neutrons"*. The observational confirmation occurred in the 1960's by J. Bell and A. Hewish (see Hewish et al., 1968); since that moment studies about NSs significantly grew up. This chapter summarizes briefly the NS main features.

1.1 Structure

The NS interior can be divided into several regions as shown in Figure 1.1. The **outer crust** is characterized by the absence of free neutrons. Its boundary lies at $\rho \simeq \rho_{nd}$ (see Shapiro & Teukolsky, 1983) which is the neutron drip density, i.e. the density beyond which atomic nuclei decay with the emission of a neutron. According to the current estimates $\rho_{nd} \sim$

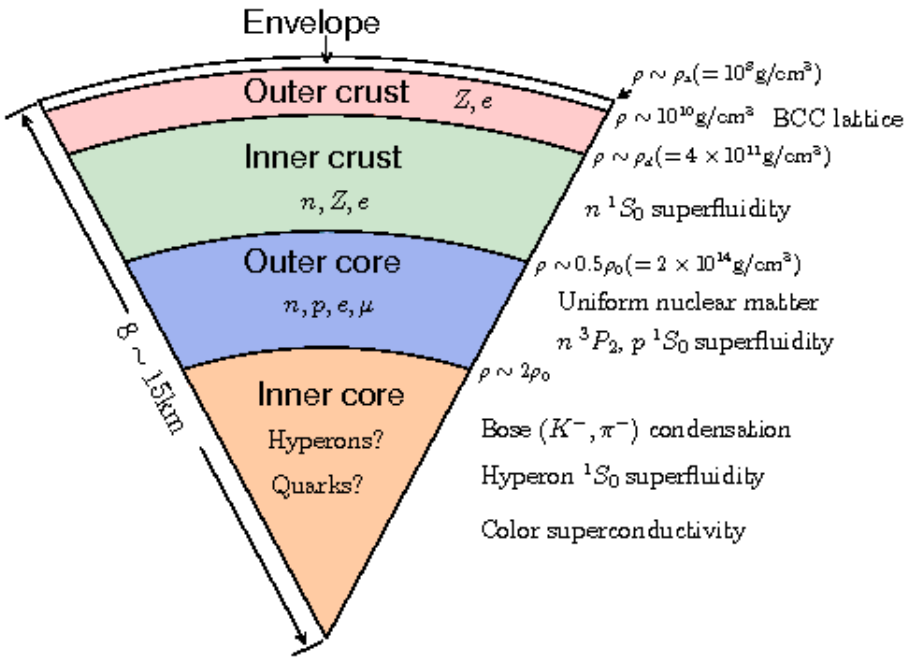

Figure 1.1: Schematic structure of a neutron star (see Lim et al., 2017).

4×10^{11} g cm^{-3}. Its matter is supposed to consist of ions and electrons and its thickness should be few hundred meters. A very thin surface layer, up to few meters in hot stars, contains a non-degenerate, almost ideal gas. The density increases going deeper in the star, where the beta capture process enriches nuclei with neutrons. At the base of the outer crust neutrons start to drip out of the nuclei producing a free neutron gas. The **inner crust** may be about one kilometer thick, with a density varying from ρ_{nd} to $\rho \sim 0.5\,\rho_0$. It is believed to be composed by electrons, free neutrons and neutron-rich atomic nuclei (Haensel, Potekhin & Yakovlev, 2007). The fraction of free neutrons increases with the growing of density. The nuclei disappear at the interface between crust and core. The **outer core** can extend up to several kilometers inside the star. It consists of a mixture between free neutrons, protons and electrons. Its density varies approximately between $0.5\,\rho_0$ and $2\,\rho_0$. Finally, the central part of the star is the **inner core**, where the density is greater than $2\,\rho_0$ and it is supposed to reach a value of $10{-}15\,\rho_0$ at the star center. The composition of the super-dense matter remains uncertain. Several hypotheses are made, such as the presence of hyperons,

the pion/kaon condensates; it has been also supposed that the matter can consist of deconfined quarks (Haensel, Potekhin & Yakovlev, 2007).

1.1.1 Atmosphere

It is believed that the NS surface may be covered by a geometrically thin **atmospheric layer**. Its thickness can be easily obtained from a trivial calculation. Considering a non relativistic ideal gas and integrating the hydrostatic equilibrium equation $dP/dr = \rho\, g$, the scale height turns out to be

$$h = \frac{k_B\, T_s}{A\, m_p\, g} \sim 10^{-1}\ \mathrm{cm}\ ,$$

where ρ is the mass density in the atmosphere, k_B is the Boltzmann constant, T_s is the surface temperature, A is the mass number of the nuclei that compose the atmosphere and m_p is the proton mass. Since the ratio h/R between the atmosphere scale height and the star radius is very small, one can safely neglect the curvature of the atmospheric layer when radiative transfer calculations are performed. The atmosphere can have different chemical compositions. The outer layers of a neutron star can consist of iron since this is the most abundant element remaining after the supernova event that gave birth to a NS. However, the outer envelopes of an isolated neutron star may also contain light elements like hydrogen and helium which comes from the outer layers of the progenitor star, ejected during the supernova event. The same occurs if matter is accreted from the surface layers of a companion star in a binary. Because of the rapid separation of ions in the strong NS gravitational field, an accreted atmosphere can consist entirely of hydrogen. If the accretion occurs at the early stages of the NS life, when the temperature is of the order of 10^7 K, the hydrogen would be burnt in thermonuclear reactions, leaving the atmosphere composed mainly by helium. In turn, some helium may be burned to form carbon.

The properties of surface emission from NS are determined by the radiative transfer in their atmosphere. Studying the emergent spectra, which can substantially differ from the Planck spectrum, it is possible to infer the surface effective temperature, the chemical composition of the atmosphere, the surface gravity and the magnetic field. NS atmospheres are different from those of normal stars due to the strong gravity and the huge magnetic field. While the former is important for all NSs, it is not so for the latter.

If the atmosphere is completely ionized, the importance of the magnetic effects depends on how large the electron cyclotron energy, $h\nu_B = heB/m_e c$ is with respect to thermal energy $k_B T$. The magnetic field can be neglect when $h\nu_B \ll k_B T$ and hence

$$B \ll (m_e\, c/h\, e)\, k_B\, T \sim 10^9 (T/10^6 \mathrm{K})\ \mathrm{G}. \tag{1.1}$$

If a substantial fraction of bound atoms is present, the electron cyclotron energy has to be compared to the binding energy. Thus the magnetic effects are determined by the ratio $h\nu_B/Z^2\mathrm{Ry} \sim (B/10^9\,)Z^{-2}$ where Z is the atomic number and $1\,\mathrm{Ry} = 13.6\,\mathrm{eV}$ is the Rydberg energy. $Z^2\mathrm{Ry}$ is the total binding energy of the atom. The magnetic effects can be neglected when the ratio $\lesssim 1$.

1.2 Neutron Star classification

NSs observed up to now in the universe can be classified into different types, according to the features they exhibit. NSs are usually represented in a P-$\dot{P}$ diagram (see Figure 1.2), by measuring their rotational periods P and time derivatives $\dot{P}$, which measure their spin-down rate (see Kaspi, 2010). From P and $\dot{P}$ it is possible to derive the characteristic age and the spin-down magnetic field intensity of each source. Typically the NS magnetic field has a dipolar form, which, written in spherical coordinates, is

$$\mathbf{B}\,(\mathbf{r}) = \frac{1}{2}\, B_p \frac{R_{NS}^3}{r^3} \left(\cos\theta\, \mathbf{e_r} + \frac{\sin\theta}{2}\, \mathbf{e}_\theta \right)\ , \tag{1.2}$$

where B_p is the magnetic field at the poles. Considering a reference system in such a way that the angular velocity of the NS, $\mathbf{\Omega}$, is parallel to the z-axis, the magnetic moment is given by

$$\mathbf{m} = \frac{1}{2} B\, R^3\, (\sin\alpha\, \cos\Omega t, \sin\alpha\, \sin\Omega t, \cos\alpha)\ , \tag{1.3}$$

where α is the angle between the angular velocity and the magnetic moment. According to the Larmor's formula, a magnetic dipole in fast rotation emits

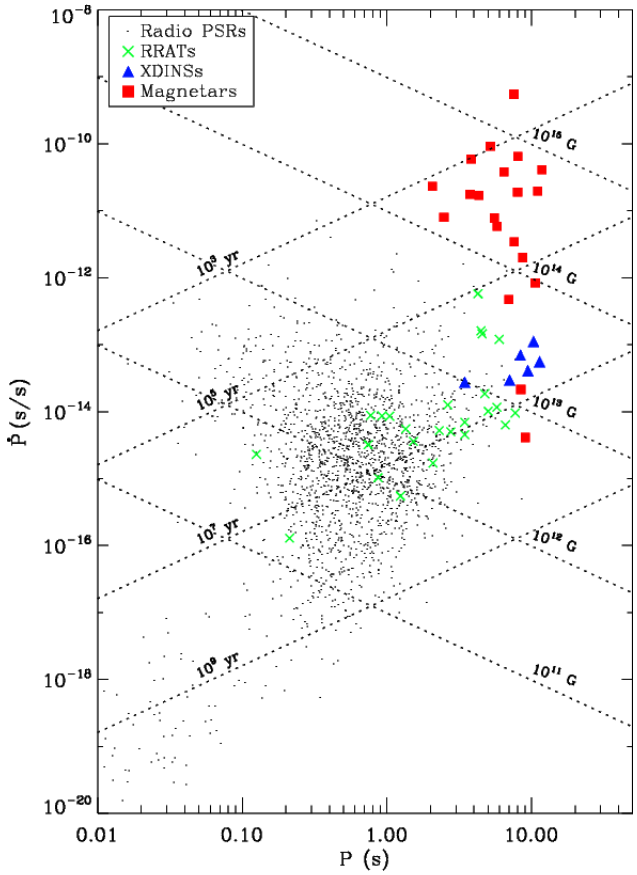

Figure 1.2: The rotational period derivative is plotted against period for radio PSRs (black dots), RRATs (green crosses), XDINSs (blue triangles) and magnetars (red squares). Dashed lines correspond to lines at constant characteristic age and inferred surface dipole magnetic field strenght.

electron magnetic radiation, with power

$$\begin{aligned}\dot{E} &= -\frac{2}{3\,c^3}\,\|\ddot{\mathbf{m}}\|^2 \\ &= -\frac{1}{6\,c^3}B^2R^6\Omega^4\sin^2\alpha\,. \end{aligned} \tag{1.4}$$

By equating the rotational energy loss rate $\dot{E} = I\Omega\dot{\Omega}$ with the emitted power (1.4) one obtains

$$\frac{\dot{\Omega}}{\Omega^3} = -\frac{B^2R^6\sin^2\alpha}{6Ic^3}\,. \tag{1.5}$$

Then, by integrating the last equation over time (from the NS birth t_0 to the present time t) and considering B, R, α and I constant in time, the characteristic age is obtained

$$t = -\frac{1}{2}\,\frac{\Omega}{\dot{\Omega}}\,, \tag{1.6}$$

where t is supposed to be much larger than t_0. The previous formula can be re-written as a function of P and $\dot{P}$ as

$$t = \frac{1}{2}\,\frac{P}{\dot{P}}\,. \tag{1.7}$$

From equation (1.5) it is possible to derive the expression of the magnetic field as a function of P and $\dot{P}$

$$B = \left(\frac{3\,I\,c^3}{2\pi^2\,R^6\,\sin^2\alpha}\,P\dot{P}\right)^{1/2} \tag{1.8}$$

and inserting typical values of the quantities ($R \sim 10^6$ cm, $I \sim 10^{45}\,\mathrm{g\,cm^2}$ and $\sin\alpha \simeq 1$ for simplicity) the expression of B turns out to be

$$B \approx 3.2 \times 10^{19}\sqrt{P\dot{P}}\ \mathrm{G}\,. \tag{1.9}$$

This values are reported in the diagram through the constant age and the constant magnetic field lines. The P-$\dot{P}$ diagram plays a similar role of the Hertzsprung-Russel diagram for ordinary stars in characterising the different NS classes. The black dots in Figure 1.2 represent **Radio Pulsars** (PSRs), which pulse regularly and predictably across the EM spectrum though generally are the most observable in the radio band. A particular subclass of pulsars are the so-called **millisecond pulsars** (placed on the bottom-left

corner in figure 1.2), which exhibit spin periods typically $\lesssim 20$ ms and very small spin-down rates. Their magnetic fields are $\lesssim 10^{10}$ G. It is believed that these rapidly-rotating NSs have been spun up through the accretion of matter from a companion star, so that millisecond pulsars are expected to be old, recycled PSRs. As the observation techniques became more advanced, it has been possible to observe NS sources with emission peaked in the X-rays, usually radio quiet and with an X-ray luminosity exceeding the rotational energy loss rate. Moreover, no companion stars or accretion disks around these objects have been observed, so that they cannot be powered by accretion as in the case of PSRs. For these reasons they were classified as **Isolated Neutron Stars** (INSs), a class that contains Magnetars, X-ray Dim Isolated Neutron Stars (XDINSs), Rotating Radio Transients (RRATs) and Central Compact Objects (CCOs). **Magnetars** are the most peculiar objects among INSs, observationally identified with Anomalous X-ray Pulsars (AXPs) and Soft Gamma-ray Repeaters (SGRs). From their values of P ($2 \div 12$ s) and $\dot{P}$ ($10^{-13} \div 10^{-10}$ s/s) it is possible to infer magnetic field intensities of the order of $B \sim 10^{14} \div 10^{15}$ G, the strongest ever detected in the universe. Alongside their persistent X-ray emission (with luminosity $L_X \sim 10^{33} \div 10^{36}$ erg/s), their most distinctive observational manifestation is the occurrence of giant/intermediate flares and short bursts, which also led to their discovery (see Turolla, Zane & Watts, 2015, for a review). Also the **XDINSs** show spin periods longer than the normal PSRs ($\mathrm{P} \sim 1 \div 10$ s) and from the values of P and $\dot{P}$ quite strong magnetic fields can be inferred ($\sim 10^{13}$ G). As for magnetars, they are observed to be radio quiet sources but do not show bursting activity. Since their characteristic ages turn out to be large ($1 \div 4$ Myr), they are believed to be old magnetars. Since 2001, exactly seven XDINSs have been detected and they are called "Magnificent Seven". The name of **RRATs** follows their peculiar emission, which contrary of PSRs show a quite irregular emission activity . This does not mean that they do not have a periodic emission but it means that a high number of nullings occur (see Burke, 2013). They are situated in unremarkable regions of the P-$\dot{P}$ diagram (Figure 1.2). The radio quiet NSs include also **CCOs** (see De Luca, 2007). They are located at the center of their supernova remnant, so they are believed to be young objects. Moreover, the values of P and $\dot{P}$ lead to very low magnetic fields, $\sim 10^{10}$ G, the lowest values inferred for INSs. For this reason they were believed to be anti-magnetars.

Chapter 2

Radiative transfer

Radiative transfer is a branch of physics which studies the propagation of radiation through a medium. Inside a star the radiation is produced by thermonuclear reactions, it travels through the interiors of the star where phenomena such as absorption, emission and scattering occur. Once reached the photosphere, radiation can travel freely or interact with interstellar medium. Radiative transfer is crucial to understand some properties of stellar astrophysics. In this thesis the interactions of radiation with matter in a neutron star atmosphere, where the emergent spectrum is formed, will be studied. The transfer equation and its consequences are the topics of this chapter.

2.1 The specific intensity, its moments and the transfer equation

The fundamental quantity that describes a radiation field is called *specific intensity* and it is defined as

$$I_\nu = \frac{dE}{d\Omega d\nu dt dA} \,, \tag{2.1}$$

i.e. the energy which crosses an infinitesimal area dA, per unit of time dt, solid angle $d\Omega$ and frequency $d\nu$. Starting from the definition (2.1) it is possible to derive the following quantities:

- *mean intensity* given by $J_\nu = (4\pi)^{-1} \int I_\nu d\Omega$;
- *monochromatic flux*, i.e. the energy passing through an area dA, in a time interval dt and in a frequency range $d\nu$, given by $F_\nu =$

$\int I_\nu \cos\theta d\Omega$ where θ is the angle between the direction of the ray and the normal to the surface;

- *momentum flux* given by $p_\nu = \int I_\nu \cos^2\theta d\Omega/c$, where c is the speed of light.

For the purposes of the following discussion, the moments of specific intensity are introduced:

$$H_\nu = \frac{1}{2}\int_{-1}^{1} I_\nu \cos\theta d\cos\theta \tag{2.2}$$

$$K_\nu = \frac{1}{2}\int_{-1}^{1} I_\nu \cos^2\theta d\cos\theta \ , \tag{2.3}$$

which are related to the energy flux and the momentum flux through constant factors, i.e. $H_\nu = (4\pi)^{-1} F_\nu$ and $K_\nu = c\ (4\pi)^{-1} p_\nu$.
The transfer equation describes how radiation can change when it travels inside a medium. In general, time variation of the radiation field properties are described by the convective derivative and depends on the emission, absorption and scattering properties of the medium. The transfer equation can be easily derived from Boltzmann equation whose expression for a gas consisting of photons is

$$\frac{Df}{Dt} = -C_{out} + C_{in} \ , \tag{2.4}$$

where $f = f(\mathbf{r}, \mathbf{n}, \nu, t)$ is the distribution function, i.e. the number of photons that are in the infinitesimal volume d^3x and that have momenta included in d^3p, $D/Dt = \partial/\partial t + \mathbf{v}\cdot\nabla$ is the convective derivative, C_{in} and C_{out} are the rates at which photons leave and enter the infinitesimal phase space volume $d^3x d^3p$. From the distribution function it is possible to derive an expression for the specific intensity. The photon number density $f d^3p$ can be re-expressed in terms of frequency

$$f d^3p = f(h/c)^3 \nu^2 d\nu d\Omega \tag{2.5}$$

using the relation $p = (h/c)\nu$ where h is the Planck constant. The number of photons which cross an infinitesimal area dA in the time dt is given by the previous expression multiplied by c. The energy which cross an infinitesimal

area dA turns out to be

$$dE = \frac{h^4\nu^3}{c^2} f d\nu d\Omega dt dA \tag{2.6}$$

and, comparing this result with equation (2.1), one obtains the relation between the specific intensity and the distribution function

$$I_\nu = \frac{h^4\nu^3}{c^2}\, f \ . \tag{2.7}$$

Inserting equation (2.7) in equation (2.4), the transfer equation turns out to be (see Mihalas, 1978, for further details)

$$\frac{1}{c}\frac{D}{Dt} I_\nu \left(\mathbf{n}, \mathbf{r}, t\right) = \eta_\nu \left(\mathbf{n}, \mathbf{r}, t\right) - \alpha_\nu \left(\mathbf{n}, \mathbf{r}, t\right) I_\nu \left(\mathbf{n}, \mathbf{r}, t\right) \ , \tag{2.8}$$

where $\eta_\nu = \eta_\nu^{ems} + \eta_\nu^s$ is the total emission coefficient, given by the sum between true emission and scattering emission, and $\alpha_\nu = \alpha_\nu^{abs} + \alpha_\nu^s$ is the total absorption coefficient, given by the sum of true absorption and scattering contributions. Actually the dependence on time can be neglected. In fact, if a region has a scale length L, photons have a time scale evolution of the order of $t_p = L/c$, while the matter contained in the region evolve with a time scale $t_m = L/v$, where v is the typical velocity of the matter. In most situations $v \ll c$, then radiation (photons) changes instantly with respect to the matter. Hence, equation (2.8) becomes

$$\frac{dI_\nu}{ds} = \eta_\nu - \alpha_\nu I_\nu \tag{2.9}$$

where s is the coordinate along the direction of the ray. Defining the *infinitesimal optical depth* $d\tau_\nu = -\alpha_\nu\, ds$, equation (2.9) can be written in the alternative form

$$\frac{dI_\nu}{d\tau_\nu} = I_\nu - S_\nu \ , \tag{2.10}$$

where $S_\nu = \eta_\nu/\alpha_\nu$ is the *source function*. Its formal solution can be easily obtained,

$$I_\nu \left(\tau_\nu\right) = I_\nu \left(\tau_1\right)\, e^{-(\tau_1 - \tau_\nu)} + \int_{\tau_\nu}^{\tau_1} d\tau'_\nu S_\nu \left(\tau'_\nu\right) e^{-(\tau'_\nu - \tau_\nu)} \ , \tag{2.11}$$

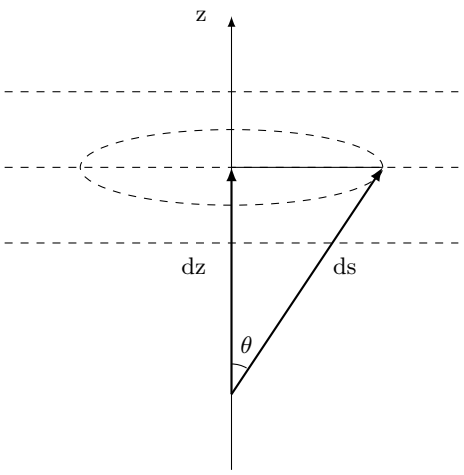

Figure 2.1: Geometry in the case of plane-parallel media. The direction of the ray is identified by **ds** and θ is the angle between the direction of the radiation and the z-axis.

where $(\tau_1, I_\nu(\tau_1))$ is the initial condition. Solving the transfer equation requires to specify of boundary conditions. Stellar atmospheres have an open boundary at one side, where it is possible to impose that there is not incident radiation at the outer layer (this is not the case of binary systems), but on the other side the atmosphere is so optically thick that it can be imagined to extend up to infinity. In this case the requirement is

$$\lim_{\tau_\nu \to \infty} I_\nu(\tau_\nu)\, e^{-\tau_\nu} = 0\,. \tag{2.12}$$

When this condition is imposed, one talks about a *semi-infinite* atmosphere. Applying the boundary condition (2.11), the solution of equation (2.12) turns out to be

$$I_\nu(\tau_\nu) = \int_{\tau_\nu}^{\infty} d\tau'_\nu S_\nu\left(\tau'_\nu\right) e^{-(\tau'_\nu - \tau_\nu)} \tag{2.13}$$

where τ_1 is replaced with infinity.

2.2 Plane parallel approximation

One talks about plane-parallel approximation when the material proprieties such as the temperature, density, pressure and others depend on a single spacial coordinate. In astrophysics this is a valid assumption in case of

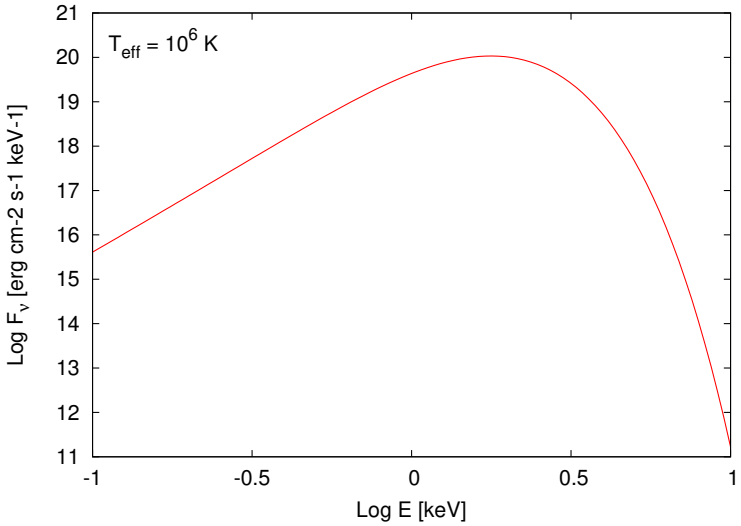

Figure 2.2: Theoretical prediction of behaviour of the monochromatic flux as a function of the photon energy in the Rosseland approximation. The temperature profile is $T(\tau_R) \simeq T_e\,(\tau_R + 2/3)^{1/4}$ and the absorption coefficient is calculated considering only bremsstrahlung (see Rybicki & Lightman, 2008).

stellar atmospheres. In this situation, the transfer equation (2.9) becomes

$$\frac{\mu}{\alpha_\nu}\frac{\partial I_\nu}{\partial z} = S_\nu - I_\nu \tag{2.14}$$

or, written as a function of the optical depth,

$$\mu\frac{\partial I_\nu}{\partial \tau_\nu} = I_\nu - S_\nu \ , \tag{2.15}$$

where $d\tau_\nu = -\alpha_\nu dz$ is the infinitesimal monochromatic optical depth, $ds = \mu\, dz$ and $\mu = \cos\theta$ is the cosine of the angle between the normal to the surface and the direction of radiation, as shown in Figure 2.1. It is useful to re-arrange the previous equation in the following form:

$$I_\nu = S_\nu - \frac{\mu}{\alpha_\nu}\frac{\partial I_\nu}{\partial z} \ . \tag{2.16}$$

If matter and photons are very close to local thermodynamic equilibrium (LTE) which occurs at large optical depths, the intensity changes slowly with the optical depth. Because the system is very close to the equilibrium, a reasonable zero-order approximation is to neglect the derivative, so that

$I_\nu^{(0)} \simeq S_\nu^{(0)} \simeq B_\nu(T)$. At the first order the intensity is obtained by replacing the terms at the right-hand side of (2.16) with their zero-order values:

$$I_\nu^{(1)} \simeq B_\nu(T) - \frac{\mu}{\alpha_\nu}\frac{\partial B_\nu}{\partial T}\frac{dT}{dz} . \tag{2.17}$$

Then, using the previous expression, the monochromatic flux turns out to be

$$F_\nu(z) = -\frac{4\pi}{3}\frac{1}{\alpha_\nu}\frac{\partial B_\nu}{\partial T}\frac{dT}{dz} \tag{2.18}$$

and the total flux, which is obtained by integrating the monochromatic flux over the frequencies,

$$F(z) = -\frac{16\,\sigma_{SB}}{3\,\alpha_R}T^3\frac{dT}{dz} , \tag{2.19}$$

where σ_{SB} is the Stefan-Boltzmann constant and α_R is the Rosseland mean absorption coefficient, such that

$$\alpha_R^{-1} = \frac{\int_0^\infty d\nu \alpha_\nu^{-1}\frac{\partial B_\nu}{\partial T}}{\int_0^\infty d\nu \frac{\partial B_\nu}{\partial T}} . \tag{2.20}$$

Equation (2.19) is called *Rosseland approximation* for the energy flux and it shows that radiative energy transport deep in a star is of the same nature as heat conduction, with effective heat conductivity equal to $16\sigma_{SB}T^3/3\alpha_R$. In can be verified that, although this result is derived in plane-parallel approximation, it holds in general.

2.3 The Schwarzschild-Milne equations

In the case of a medium with plane-parallel (or cylindrical) symmetry, it is possible to obtain the expressions of the mean intensity and flux. These relations are called *Schwarzschild-Milne equations*. Using the boundary condition of a semi-infinite atmosphere (2.15), the formal solution of equation (2.12) is

$$I_\nu(\tau_\nu) = \frac{1}{\mu}\int_{\tau_\nu}^\infty d\tau'_\nu S_\nu(\tau'_\nu)\, e^{-\frac{(\tau'_\nu-\tau_\nu)}{\mu}} . \tag{2.21}$$

Using the previous expression, the mean intensity becomes

$$\begin{aligned} J_\nu(\tau_\nu) &= \frac{1}{2}\int_{-1}^{1} I_\nu(\tau_\nu,\mu)\, d\mu \\ &= \frac{1}{2}\left[\int_0^1 d\mu \int_{\tau_\nu}^{\infty} S_\nu(t)\, e^{-\frac{t-\tau_\nu}{\mu}}\, \frac{dt}{\mu}\right. \\ &\left. + \int_{-1}^{0} d\mu \int_0^{\tau_\nu} S_\nu(t)\, e^{-\frac{\tau_\nu - t}{-\mu}}\, \frac{dt}{-\mu}\right] . \end{aligned} \tag{2.22}$$

Performing a substitution $w = \pm 1/\mu$ the previous equation turns out to be

$$\begin{aligned} J_\nu(\tau_\nu) &= \frac{1}{2}\int_{-1}^{1} I_\nu(\tau_\nu,\mu)\, d\mu \\ &= \frac{1}{2}\left[\int_0^1 d\mu \int_{\tau_\nu}^{\infty} S_\nu(t)\, e^{-\frac{t-\tau_\nu}{\mu}}\, \frac{dt}{\mu}\right. \\ &\left. + \int_{-1}^{0} d\mu \int_0^{\tau_\nu} S_\nu(t)\, e^{-\frac{\tau_\nu - t}{-\mu}}\, \frac{dt}{-\mu}\right] . \end{aligned} \tag{2.23}$$

Equation (2.23) can be written in a simpler form

$$J_\nu(\tau_\nu) = \frac{1}{2}\int_0^{\infty} S_\nu(t)\, E_1|t-\tau_\nu|\, dt\ , \tag{2.24}$$

where $E_1(x) = \int_1^\infty e^{-x\,t} dt/t$ is the first exponential integral. In general, for any positive integer n, the n-th exponential integral is defined as

$$E_n(x) = \int_1^{\infty} t^{-n}\, e^{-x\,t}\, dt \tag{2.25}$$

or in an equivalent form

$$E_n(x) = x^{n-1}\int_x^{\infty} t^{-n}\, e^{-t}\, dt\ . \tag{2.26}$$

Equation (2.24) was first discovered by Schwarzschild (see Schwarzschild, 1914).

The flux can be derived similarly

$$\begin{aligned} F_\nu(\tau_\nu) &= 2\pi \int_{-1}^{1} I_\nu(\tau_\nu, \mu)\ \mu\, d\mu \\ &= 2\pi \left[\int_0^1 d\mu \int_{\tau_\nu}^{\infty} S_\nu(t)\ e^{-\frac{t-\tau_\nu}{\mu}}\, dt \right. \\ &\left. + \int_{-1}^{0} d\mu \int_0^{\tau_\nu} S_\nu(t)\ e^{-\frac{\tau_\nu - t}{\mu}}\, dt \right] , \end{aligned} \tag{2.27}$$

and, as in the case of the mean intensity, the final expression is

$$F_\nu(\tau_\nu) = 2\pi \left[\int_{\tau_\nu}^{\infty} dt\, S_\nu(t)\, E_2(t - \tau_\nu) - \int_0^{\tau_\nu} dt\, S_\nu(t)\ E_2(\tau_\nu - t) \right] . \tag{2.28}$$

It is important to stress that the formal solution of the transfer equation is indeed only formal and its simplicity is illusory. In general the source function contains scattering terms which include the mean intensity in their expressions. Therefore it is clear that the source function, which is required to compute the radiation field, depends itself on the radiation field. One of the possible way to find solutions to the transfer problem is to make some assumptions, compute the results and use a correction procedure. This is the approach that has been used in this thesis.

2.4 The polarized transfer equations

Strong magnetic fields can alter the properties of the medium in which photons propagate. In particular, photons are expected to be linearly polarized in two normal modes, the ordinary and the extraordinary ones, in which their electric field oscillates either parallel or perpendicular to the $\hat{\mathbf{k}}\,\mathbf{B}$ plane, with $\hat{\mathbf{k}}$ the photon propagation direction and $\mathbf{B}$ the star magnetic field. In this case, to solve the radiative transfer equation is convenient to introduce the polarization matrix (see Mészáros, 1992)

$$\rho_{\alpha\beta} \propto \begin{pmatrix} \langle E_x E_x \rangle & \langle E_x E_y \rangle \\ \langle E_y E_x \rangle & \langle E_y E_y \rangle \end{pmatrix} , \tag{2.29}$$

where E_x, E_y are the photon electric field along two orthogonal arbitrary directions in the plane orthogonal $\hat{\mathbf{k}}$. If the refractive index of the medium, n, is close to unity, then the transfer equation can be written in the form

(see Gnedin & Pavlov, 1974)

$$\left(\hat{\mathbf{k}}\cdot\nabla\right)\rho_{\alpha\beta} = -\frac{1}{2}\sum_{\gamma}\left(T_{\alpha\gamma}\rho_{\gamma\beta} + \rho_{\alpha\gamma}T^{\dagger}_{\gamma\beta}\right) + S_{\alpha\beta}, \tag{2.30}$$

where $T_{\alpha\beta}$ is the transfer matrix, in which the hermitian and the anti-hermitian part describe respectively the absorption of radiation and the transition from one polarization state to the other and $S_{\alpha\beta}$ is a source term which describes the scattering emission and the emission mechanisms (Mészáros, 1992). $S_{\alpha\beta}$ includes also an integral term depending on $\rho_{\alpha\beta}$. The basis vector used to describe $\rho_{\alpha\beta}$ and $T_{\alpha\beta}$ are an arbitrary set of $\mathbf{e_x}$, $\mathbf{e_y}$ and $\mathbf{e_z}$. It is possible to find the eigenvectors of $T_{\alpha\beta}$, $\mathbf{e_j}$, of components $e_{\alpha\,j}$, and their eigenvalues, T_j, with $j = 1, 2$. The index j describes normal modes: $j = 1$ corresponds to the extraordinary wave while $j = 2$ the ordinary one. The real and the imaginary part of T_j describe the absorption coefficient α_j and refractive index $\omega\, n_j/c$ for the j-th wave, respectively. The transfer equation, expressed in the normal wave representation, turns out to be

$$\left(\hat{\mathbf{k}}\cdot\nabla\right)R_{jk} = -g_{jk}R_{jk} + S_{jk}\,. \tag{2.31}$$

Here

$$g_{jk} = \frac{T_j + T_k^{\dagger}}{2} = \frac{\alpha_j + \alpha_k}{2} + i\omega\frac{n_j - n_k}{c} \tag{2.32}$$

$$S_{jk} = (e_{j\alpha})^{-1}\, S_{\alpha\beta}\left(e^{\dagger}_{k\beta}\right)^{-1} \tag{2.33}$$

$$R_{jk} = (e_{j\alpha})^{-1}\, \rho_{\alpha\beta}\left(e^{\dagger}_{k\beta}\right)^{-1} \tag{2.34}$$

are respectively the transfer matrix, the source term and the density matrix in the normal wave representation. The diagonal elements of the density matrix represent the intensities of the normal waves, $R_{ii} = I_i$. The source matrix can depend on R_{ij} (Mészáros, 1992) and therefore equation (2.31) represents a set of four coupled equations. The formal solution of equation (2.31) is

$$\begin{aligned} R_{jk}(z) = {} & R_{jk}(z_0)\exp\left[-\int_{z_0}^{z} g_{jk}\left(z'\right)dz'\right] \\ & + \int_{z_0}^{z} S_{jk}(z_1)\exp\left[-\int_{z_1}^{z} g_{jk}\left(z'\right)dz'\right]dz'\,, \end{aligned} \tag{2.35}$$

where z is the coordinate along the direction of the wave $\hat{\mathbf{k}}$ and z_0 is sthe lower limit of the integration integral. In the right-hand side of equation (2.35), the exponential in the second term gives a significant contribution when the real part of the exponent is smaller than 1. If $\mathrm{Im}\left(\int_{z_1}^{z} g_{jk}\left(z'\right) dz'\right) \gg \mathrm{Re}\left(\int_{z_1}^{z} g_{jk}\left(z'\right) dz'\right)$ or, for a homogeneous medium, $\omega\left(n_j - n_k\right)/c \gg \left(\alpha_j + \alpha_k\right)/2$, the integral for $j \neq k$ is suppressed with respect to that for $j = k$ because of the rapidly oscillating factor. For circular polarization modes, this condition is called large Faraday depolarization. In this case, equation (2.31) can be written as

$$\left(\hat{\mathbf{k}} \cdot \nabla\right) R_{jk} = -g_{jk} R_{jk} + S_{jj}\delta_{jk}\,, \tag{2.36}$$

where the non-diagonal elements of the above equation are damped out over a distance $\sim 2/(\alpha_j + \alpha_k)$. Then, equation (2.36) becomes

$$\begin{aligned}\left(\hat{\mathbf{k}} \cdot \nabla\right) I_\nu^j\left(\mathbf{k}\right) =& \rho\kappa_j^{abs}\left(\mathbf{k}\right)\frac{B_\nu}{2} - \rho\kappa_j^{tot}\left(\mathbf{k}\right) I_\nu\left(\mathbf{k}\right) \\ &+ \rho\sum_{j=1,2}\int d\Omega' \frac{d\kappa^s\left(\mathbf{k}'^i \rightarrow \mathbf{k}^j\right)}{d\Omega} I_\nu^i\left(\mathbf{k}'\right)\,,\end{aligned} \tag{2.37}$$

where κ_j^{abs} is the absorption opacity, $d\kappa^s/d\Omega$ is the differential opacity for scattering from mode i in direction $\mathbf{k}'$ to mode j in direction $\mathbf{k}$ and $\kappa_j^{tot} = \kappa_j^{abs} + \kappa_j^s$ is the total opacity (see Ho & Lai, 2001). In plane-parallel approximation, equation (2.37) becomes

$$\begin{aligned}\mu\frac{\partial I_\nu^j\left(\mathbf{k}\right)}{\partial\tau} =& \frac{\kappa_j^{tot}\left(\mathbf{k}\right)}{\kappa_0^s} I_\nu^j\left(\mathbf{k}\right) - \frac{\kappa_j^{abs}\left(\mathbf{k}\right)}{\kappa_0^s}\frac{B_\nu}{2} \\ &- \frac{1}{\kappa_0^s}\sum_{i=1,2}\int d\Omega' \frac{d\kappa^s\left(\mathbf{k}'^i \rightarrow \mathbf{k}^j\right)}{d\Omega} I_\nu^i\left(\mathbf{k}'\right)\,,\end{aligned} \tag{2.38}$$

where $\mu = \hat{\mathbf{k}} \cdot \hat{\mathbf{z}} = \cos\theta$, $d\tau = -\rho k_0^s dz$ is the infinitesimal Thomson optical depth, $\kappa_0^s = \sigma_T n_e/\rho$ is the Thomson scattering opacity and σ_T is the Thomson cross section. In order to solve the radiative transfer equation, it is convenient to introduce the symmetric and the anti-symmetric part of the

specific intensity I_ν with respect to μ

$$i_\nu^j(\mathbf{k}) = \frac{1}{2}\left[I_\nu^j(\mathbf{k}) + I_\nu^j(-\mathbf{k})\right] \tag{2.39}$$

$$f_\nu^j(\mathbf{k}) = \frac{1}{2}\left[I_\nu^j(\mathbf{k}) - I_\nu^j(-\mathbf{k})\right] , \tag{2.40}$$

where $\mu \geq 0$. From equation (2.38), it is possible to write the radiative transfer equation in terms of i_ν^j and f_ν^j

$$f_\nu^j(\mathbf{k}) = \mu\frac{\partial i_\nu^j(\mathbf{k})}{\partial\tau_\nu} \tag{2.41}$$

$$\begin{aligned}\mu^2\frac{\partial^2 i_\nu^j(\mathbf{k})}{\partial\tau_\nu^2} = {} & i_\nu^j(\mathbf{k}) - \frac{\kappa_j^{abs}(\mathbf{k})}{k_j^{tot}(\mathbf{k})}\frac{B_\nu}{2} \\ & - \frac{2}{\kappa_j^{tot}(\mathbf{k})}\sum_{i=1,2}\int_{\mu\geq 0} d\Omega'\frac{d\kappa^s(\mathbf{k}'_\mathbf{i}\to\mathbf{k}_j)}{d\Omega}i_\nu^i(\mathbf{k}') .\end{aligned} \tag{2.42}$$

The reflection symmetry of the opacity is used to derive the above equations (see Ho & Lai, 2001). The boundary conditions for (2.42) are (see Mihalas, 1978)

$$\mu\frac{\partial i_\nu^j}{\partial\tau_\nu} = i_\nu^j \quad \text{at } \tau_\nu = 0 \tag{2.43}$$

$$\mu\frac{\partial i_\nu^j}{\partial\tau_\nu} + i_\nu^j = \frac{1}{2}\left(\mu\frac{\partial B_\nu}{\partial\tau_\nu} + B_\nu\right) \quad \text{at } \tau_\nu \to \infty . \tag{2.44}$$

The integration of equation (2.37) over the solid angle gives

$$\begin{aligned}\nabla\cdot\mathbf{F}_\nu^j(\mathbf{k}) = {} & \rho\int d\Omega\,\kappa_j^{abs}(\mathbf{k})\frac{B_\nu}{2} - \rho\int d\Omega\,\kappa_j^{tot}(\mathbf{k})\,I_\nu^j(\mathbf{k}) \\ & - \rho\sum_{i=1,2}\int d\Omega\int d\Omega'\frac{d\kappa^s(\mathbf{k}'_i\to\mathbf{k}_j)}{d\Omega}I_\nu^i(\mathbf{k}')\end{aligned} \tag{2.45}$$

In order to derive the radiative transfer equations in diffusion approximation, it is convenient to get a formula for the energy flux. Multiplying equation (2.37) by a factor $-\mathbf{k}/\rho\kappa_j^{tot}(\mathbf{k})$ and integrating over the solid angle, one obtains

$$\mathbf{F}_\nu^j = -\int d\Omega\,\frac{1}{\rho\kappa_j^{tot}(\mathbf{k})}\mathbf{k}\,(\mathbf{k}\cdot\nabla)\,I_\nu^j(\mathbf{k}) , \tag{2.46}$$

exploiting the reflection symmetry. In the diffusion limit the specific intensity is approximated as $I_\nu^j \simeq (c/4\pi)\left[u_\nu^j + (3/c)\,\mathbf{k}\cdot\mathbf{F}_\nu^j\right]$, where $u_\nu^j =$

$(4\pi/c)J^j_\nu$. Using the fact that $\nabla u^j_\nu = \left(\partial u^j_\nu/\partial z\right)\mathbf{e_z}$ and that the opacity depends on $\mu_B = \hat{\mathbf{k}}\cdot\hat{\mathbf{B}} = \cos\theta_B$, equation (2.46) becomes

$$\mathbf{F}^j_\nu \sim -c\frac{\partial u^j_\nu}{\partial z}\left(l^{\parallel}_j \cos\Theta_B \hat{\mathbf{B}} + l^{\perp}_j \sin\Theta_B \hat{\mathbf{B}}_\perp\right) , \tag{2.47}$$

where $\hat{\mathbf{B}}_\perp$ is a unit vector perpendicular to be $\mathbf{B}$ which lies on the plane of $\hat{\mathbf{B}}$ and $\mathbf{e_z}$, Θ_B is the angle between $\mathbf{e_z}$ and B, $l^{\parallel}_j$ and $l^{\perp}_j$ are the angle-average mean free path parallel and perpendicular respectively to the magnetic field

$$l^{\parallel}_j = \int_0^1 d\mu_B \frac{\mu_B^2}{\rho\kappa^{tot}_j(\mu_B)} \tag{2.48}$$

$$l^{\perp}_j = \int_0^1 d\mu_B \frac{1-\mu_B^2}{\rho\kappa^{tot}_j(\mu_B)} . \tag{2.49}$$

Along $\mathbf{e_z}$ the average mean free path is

$$l_j = l^{\parallel}_j \cos^2\Theta_B + l^{\perp}_j \sin^2\Theta_B \tag{2.50}$$

and the specific flux is

$$F^j_{\nu,z} \sim -c\, l_j \frac{\partial u^j_\nu}{\partial z} . \tag{2.51}$$

From equation (2.45), it is possible to obtain the two radiation transport equations in the diffusion approximation inserting the approximated formula for intensity and the energy flux

$$\frac{\partial}{\partial\tau}\left(\frac{l_j}{l_0}\frac{\partial u^j_\nu}{\partial\tau}\right) = \frac{K^{abs}_j}{\kappa^s}\left(u^j_\nu - \frac{u^P_\nu}{2}\right) + \frac{K^s_{21}}{\kappa^s}\left(u^j_\nu - u^{3-j}_\nu\right) , \tag{2.52}$$

where $u^P_\nu = (4\pi/c)B_\nu$ is the blackbody energy density, $l_0 = (n_e\sigma_T)^{-1}$ is the mean free path before a Thomson scattering occurs and

$$K^{abs}_j = \frac{1}{4\pi}\int d\Omega\, \kappa^{abs}_j(\mathbf{k}) \tag{2.53}$$

$$K^{tot}_j = \frac{1}{4\pi}\int d\Omega\, \kappa^{tot}_j(\mathbf{k}) \tag{2.54}$$

$$K^s_{ij} = \frac{1}{4\pi}\int d\Omega\, \kappa^s_{ij}(\mathbf{k}) . \tag{2.55}$$

The boundary conditions are

$$\frac{l_j}{l_0}\frac{\partial u_\nu^j}{\partial \tau} = \frac{u_\nu^j}{2} \quad \text{at } \tau = 0 \tag{2.56}$$

$$\frac{\partial u_\nu^j}{\partial \tau} + u_\nu^j = \frac{1}{2}\left(\frac{\partial u_\nu^P}{\partial \tau} + u_\nu^P\right) \quad \text{at } \tau \to \infty\,. \tag{2.57}$$

Chapter 3

Neutron Star atmosphere model

Thermal radiation from the NS surface provides important information about these compact objects. Observations of the thermal surface emission from NSs allow the direct measurement of fundamental NS properties, such as their effective temperatures, their atmospheric abundances and their surface gravity. The first NS atmosphere model involving realistic opacities was developed by Romani (1987) using atomic data from Los Alamos Opacity Library (Huebner et al., 1977). Following works, such as Rajagopal & Romani (1996), Zavlin et al. (1996) or Gänsicke et al. (2002), include different atomic data released from OPAL (Iglesias & Rogers, 1992) or OP project (Seaton et al., 1994).
The atmosphere model is built under the following assumptions.

Assumption 1: plane-parallel geometry. In the case of NSs, the atmosphere scale height, $h \lesssim 10$ cm, is very small compared to the radius, $R \sim 10$ km, hence the curvature is negligible.

Assumption 2: hydrostatic equilibrium.

Assumption 3: radiative equilibrium. The atmosphere does not contain sources of energy.

Assumption 4: local thermal equilibrium (LTE).

This chapter is divided into three main topics. In section 3.1 the implication of radiative equilibrium is discussed. In section 3.2 and 3.3 the grey atmosphere and the Lucy-Unsöld correction procedure, which are necessary for the construction of the atmosphere model, are introduced. In section 3.4

the full theoretical model is presented.

3.1 Radiative equilibrium

Energy can be trasported either though the radiative channel or through the convective one. When the energy is transported only by the radiative mode, one talks about *radiative equilibrium*. Analogously when energy is transferred only by convective mode, one talks about *convective equilibrium*. The radiative equilibrium has as a consequence that the total energy flux is constant. In order to show this result, one can integrate equation (2.8) over the solid angle, obtaining

$$\frac{4\pi}{c}\frac{\partial J_\nu(\mathbf{r},t)}{\partial t}+\nabla\cdot F_\nu(\mathbf{r},t) = \int_{4\pi}\left[\eta_\nu(\mathbf{r},\mathbf{n},t)-\alpha_\nu(\mathbf{r},\mathbf{n},t)\ I_\nu(\mathbf{r},\mathbf{n},t)\right]d\Omega\ . \tag{3.1}$$

The integration of equation (3.1) over the frequencies gives the *energy equation* for a radiation field

$$\frac{\partial E_R(\mathbf{r},t)}{\partial t}+\nabla\cdot F(\mathbf{r},t) = \int_0^\infty\int_{4\pi}\left[\eta_\nu(\mathbf{r},\mathbf{n},t)-\alpha_\nu(\mathbf{r},\mathbf{n},t)\ I_\nu(\mathbf{r},\mathbf{n},t)\right]d\Omega\,d\nu\ , \tag{3.2}$$

where E_R is the radiation energy density. The previous equation has a simple physical interpretation: the time rate of change of radiation energy is equal to the difference between the total energy emitted and absorbed by the medium. If the emission and absorption coefficients are angle independent, then equation (3.2) becomes

$$\frac{\partial E_R(\mathbf{r},t)}{\partial t}+\nabla\cdot F(\mathbf{r},t) = 4\pi\int_0^\infty\left[\eta_\nu(\mathbf{r},t)-\alpha_\nu(\mathbf{r},t)\ J_\nu(\mathbf{r},\mathbf{n},t)\right]d\nu\ . \tag{3.3}$$

Assuming that the total emission and absorption coefficients are angle-independent implies:

$$\int_0^\infty d\nu\int_{4\pi}d\Omega\,\alpha_\nu(\mathbf{r})\ I_\nu(\mathbf{r}) = 4\pi\int_0^\infty d\nu\,\alpha_\nu(\mathbf{r})\,J_\nu(\mathbf{r}) \tag{3.4}$$

$$\int_0^\infty d\nu\int_{4\pi}d\Omega\,\eta_\nu(\mathbf{r}) = 4\pi\int_0^\infty d\nu\,\alpha_\nu(\mathbf{r})\ S_\nu(\mathbf{r})\ , \tag{3.5}$$

where in equation (3.5) the expression of the source function $S_\nu = \eta_\nu/\alpha_\nu$ was used. The radiative equilibrium means that the total energy emitted is equal to the total energy absorbed in a given volume dV and in the time dt; thus at each depth in the atmosphere

$$4\pi \int_0^\infty d\nu\, \eta_\nu(\mathbf{r}) = 4\pi \int_0^\infty d\nu\, \alpha_\nu(\mathbf{r})\; J_\nu(\mathbf{r}) \tag{3.6}$$

$$4\pi \int_0^\infty d\nu\, [\eta_\nu(\mathbf{r}) - \alpha_\nu(\mathbf{r})\; J_\nu(\mathbf{r})] = 0 \tag{3.7}$$

$$4\pi \int_0^\infty d\nu\, \alpha_\nu(\mathbf{r})\, [S_\nu(\mathbf{r}) - J_\nu(\mathbf{r})] = 0\,. \tag{3.8}$$

Inserting equation (3.7) in the expression (3.3), the implication of radiative equilibrium yields

$$\nabla \cdot \mathbf{F} = 0\,, \tag{3.9}$$

if the radiation field is time-independent. Equation (3.9) means that the total flux is constant.

Due to its invariance, the total flux can be used as a parameter that describes the atmosphere. An equivalent quantity often employed is the *effective temperature* T_{eff}, i.e. the temperature of the atmosphere if radiation were planckian

$$F = F_{eff} = \int_0^\infty d\nu\, F_\nu = \sigma_{SB} T_{eff}^4\,. \tag{3.10}$$

3.2 Grey Atmosphere

In a *grey atmosphere* the monochromatic opacity $k_\nu = \alpha_\nu/\rho$ and the emissivity $\epsilon_\nu = \eta_\nu/\rho$ of the material that composes the atmosphere are assumed to be independent on the frequency:, i.e. $k_\nu = k$ and $\epsilon_\nu = \epsilon$. The standard planar (*assumption 1*) equation of transfer (2.14) integrated over the frequencies gives

$$\mu \frac{\partial I}{\partial \tau} = I - S\,. \tag{3.11}$$

In the following the quantities without the subscript ν indicate frequency-integrated quantities, e.g. $I = \int d\nu I_\nu$ and $S = \int d\nu S_\nu$. From the *assumption 3*, equation (3.8) implies the equality between the source function and the

mean intensity. Therefore equation (3.11) becomes

$$\mu \frac{\partial I}{\partial \tau} = I - J \ , \tag{3.12}$$

the formal solution of which is

$$J(\tau) = \frac{1}{2} \int_0^\infty dt \, J(t) \, E_1(|t - \tau|) \ . \tag{3.13}$$

Kirchhoff's theorem ensures that $S = B$ if the atmosphere is in LTE (*assumption 4*) . This implies

$$J(\tau) = S(\tau) = B(\tau) = \frac{\sigma_{SB} \, T(\tau)^4}{\pi} \ . \tag{3.14}$$

Integrating equation (3.11) over μ yields

$$\frac{d\,H}{d\tau} = J - S \ , \tag{3.15}$$

where H is the first moment of the specific intensity, defined in (2.2). From *assumption 3*, one knows that the total flux, i.e. the first moment of the intensity, is constant at each depth in the atmosphere. From equation (3.15) one finds the same result. Moreover multiplying equation (3.11) by an extra factor μ and integrating over μ gives a differential equation for the second moment of the specific intensity K (defined in equation 2.3)

$$\frac{dK}{d\tau} = H \ . \tag{3.16}$$

Upon integration, the previous expression yields

$$K = H\,\tau + C = H(\tau + q) \ \ , \tag{3.17}$$

where C is a constant of integration and $q = C/H$. In general q is a function of τ and it is called *Hopf function*. If the specific intensity is isotropic the flux of momentum can be written in terms of the mean intensity, $p = (4\pi/3c)\,J$. From $p = (4\pi/c)\,K$ it is possible to obtain a relation between K and the Planck's law

$$K = \frac{1}{3}\,J = \frac{1}{3}\,B \ . \tag{3.18}$$

By substituting equation (3.18) in equation (3.17) one obtains

$$B = \frac{3}{4\pi} F_{eff} \left(\tau + q\right) \tag{3.19}$$

and it is possible to derive the temperature profile using the relations

$$B = \frac{\sigma_{SB}\, T\left(\tau\right)^4}{\pi}, \quad F_{eff} = \sigma_{SB}\, T_{eff}^4 \ . \tag{3.20}$$

Therefore the temperature profile is given by

$$T\left(\tau\right)^4 = \frac{3}{4}\, T_{eff}^4 \ \left(\tau + q\right) \ . \tag{3.21}$$

Then using the formal solution (2.21), the specific intensity at $\tau = 0$ turns out to be

$$I\left(\tau = 0, \mu\right) = \frac{3}{4\pi}\, F_{eff} \ \left(\mu + q\right) \ , \tag{3.22}$$

where the source function S has been replaced with B using the equation (3.19). Using the definition of flux, the previous result gives

$$\begin{aligned} F_{eff} &= 2\pi \int_{-1}^{1} I\left(\tau = 0, \mu\right) \ \mu \, d\mu \\ &= F_{eff} \left(\frac{1}{2} + \frac{3}{4} q\right) \end{aligned} \tag{3.23}$$

and solving this equation the value of q can be found

$$q = \frac{2}{3} \ . \tag{3.24}$$

Finally, the temperature profile of a grey atmosphere is given by

$$T\left(\tau\right)^4 = \frac{3}{4}\, T_{eff}^4 \ \left(\tau + \frac{2}{3}\right) \ . \tag{3.25}$$

The behaviour of T as a function of the optical depth is shown in Figure 3.1. At small values of τ the temperature is almost constant while at high values it goes as $\tau^{1/4}$. *Assumption 3*, radiative equilibrium, sets boundaries to the effective temperature. In fact if the effective temperature is sufficiently high, then chemical elements that compose the atmosphere would be burnt and then there would be another source of energy, e.g. in the case of hydrogen atmosphere at $\log T_{eff}[K] = 6.5$ (blue line in Figure 3.25), hydrogen would

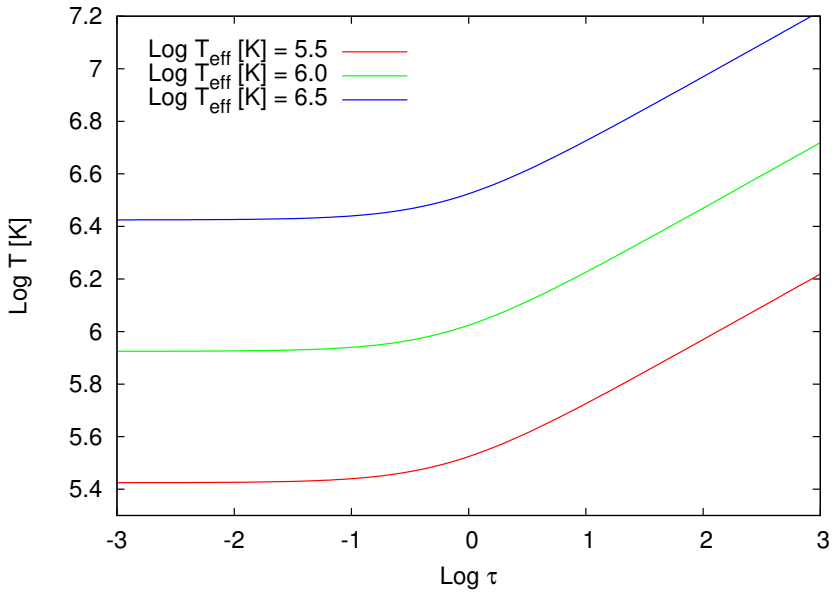

Figure 3.1: Temperature profile as a function of the optical depth for different values of the effective temperature T_{eff}.

be burnt at a temperature $\sim 10^7$ K, which is reached at $\tau \sim 100$.

3.3 The correction procedure

One of the methods used to solve the transfer equation is through an iterative scheme, which implies the construction of a correction procedure. One makes a first initial guess, then computes the results through which the corrections are re-calculated. The results are re-computed and so on until convergence, which occurs when radiative equilibrium is reached. In this thesis the solution of the transfer equation starts from the approximation of a grey atmosphere which is clearly incorrect because the atmosphere is non-grey. This approximation involves the temperature profile, so the correction procedure has to be written for the temperature. In this section two procedures will be presented: the Unsöld procedure and the Lucy-Unsöld procedure. The first one considers the opacity and the emissivity of the material as independent from the frequency (grey case) while the second one is a generalization to the non-grey case.

3.3.1 The Unsöld procedure

The basic idea is to start from an initial estimate of the source function $S(\tau) = B(\tau)$, for which the radiative equilibrium is not satisfied, and to derive a perturbation equation for $\Delta B(\tau)$ from which the perturbation equation for the temperature can be computed. If the flux is calculated from the initial guess $B(\tau)$, it will not be exactly constant but it will rather depend on the optical depth, unless $B(\tau)$ is the exact solution to the problem. In general the solution of equation (3.16) is

$$K(\tau) = \int_0^\tau H\left(\tau'\right)\, d\tau' + C\,, \tag{3.26}$$

where $C = K(0)$ is the integration constant. Considering the relation $J(\tau) = 3K(\tau)$ and taking C in such a way that $3\,C = J(0) = 2\,H(0)$, it is possible to obtain an equation for the mean intensity

$$J(\tau) = 3\int_0^\tau H\left(\tau'\right)\, d\tau' + 2\,H(0)\ , \tag{3.27}$$

which can be inserted in the following equation

$$B(\tau) = J(\tau) - \frac{dH(\tau)}{d\tau} \tag{3.28}$$

obtaining

$$B(\tau) = 3\int_0^\tau H\left(\tau'\right)\, d\tau' + 2\,H(0) - \frac{dH(\tau)}{d\tau}\ . \tag{3.29}$$

Then, introducing the correction to the source function $\Delta B(\tau)$, if the flux computed from the new source function $B(\tau) + \Delta B(\tau)$ is constant one gets

$$B(\tau) + \Delta B(\tau) = 3\int_0^\tau H_{eff}\, d\tau' + 2H_{eff}\ . \tag{3.30}$$

Subtracting (3.29) from (3.30) the correction $\Delta B(\tau)$ is given by

$$\Delta B(\tau) = 3\int_0^\tau \Delta H\left(\tau'\right)\, d\tau' + 2\Delta H(\tau) - \frac{d\Delta H(\tau)}{d\tau}\,, \tag{3.31}$$

where $\Delta H(\tau) = H_{eff} - H(\tau)$. Equation (3.31) can be written as a perturbation equation for the temperature profile with the help of the following

relations

$$\Delta B(\tau) = \frac{4\,\sigma_{SB}}{\pi} T(\tau)^3\ \Delta T(\tau)\ , \tag{3.32}$$

$$H(\tau) = \frac{1}{4\pi} F(\tau)\ . \tag{3.33}$$

In this way the perturbation equation for the temperature profile turns out to be

$$\Delta T(\tau) = \frac{1}{16\,\sigma_{SB}\,T(\tau)^3}\left[3\int_0^\tau \Delta F\left(\tau'\right)\,d\tau' + 2\,\Delta F(0) - \frac{d\Delta F(\tau)}{d\tau}\right], \tag{3.34}$$

where $\Delta F(\tau) = F_{eff} - F(\tau)$.

3.3.2 The Lucy-Unsöld procedure

The procedure presented in the previous section can be generalized to the case in which the opacity and the emissivity depend on the frequency. The correction procedure which follows from this consideration is called *Lucy-Unsöld procedure*. The equation, obtained by dividing equation (2.9) by the Rosseland mean opacity $\kappa_R = \alpha_R/\rho$, is

$$\mu\,\frac{dI_\nu}{d\tau_R} = \frac{\kappa_\nu}{\kappa_R}\,(I_\nu - B_\nu)\ , \tag{3.35}$$

where τ_R is the *Rosseland mean optical depth* and $d\tau_R = -\alpha_R dz$. The integration over μ gives

$$\frac{dH_\nu}{d\tau_R} = \frac{\kappa_\nu}{\kappa_R}\,J_\nu - \frac{\kappa_\nu}{\kappa_R}\,B_\nu\ . \tag{3.36}$$

Integrating the previous expression over the frequencies, one obtains

$$B = \frac{\kappa_J}{\kappa_P}\,J - \frac{\kappa_R}{\kappa_P}\,\frac{dH}{d\tau_R}\ . \tag{3.37}$$

Here

$$\kappa_J(\tau_R) = \frac{\int_0^\infty d\nu J_\nu(\tau_R)\ \kappa_\nu(\tau_R)}{J(\tau_R)} \tag{3.38}$$

is the *absorption mean opacity* and

$$\kappa_P(\tau_R) = \frac{\int_0^\infty d\nu B_\nu(\tau_R)\ \kappa_\nu(\tau_R)}{B(\tau_R)} \tag{3.39}$$

is the *Planck mean opacity*. Integrating equation (3.35), multiplied by an extra factor μ, over μ gives a differential equation for K_ν

$$\frac{dK_\nu}{d\tau_R} = \frac{\kappa_\nu}{\kappa_R} H_\nu \ . \tag{3.40}$$

Upon a further integration over frequencies, one gets

$$\frac{dK(\tau_R)}{d\tau_R} = \frac{\kappa_F}{\kappa_R} H(\tau_R) \ , \tag{3.41}$$

where

$$\kappa_F(\tau_R) = \frac{\int_0^\infty d\nu F_\nu(\tau_\nu)\,\kappa_\nu(\tau_R)}{F(\tau_R)} \ . \tag{3.42}$$

is the *flux mean opacity*. Solving equation (3.41) yields

$$K(\tau_R) = \int_0^{\tau_R} \frac{\kappa_F(\tau')}{\kappa_R(\tau')} H(\tau')\ d\tau' + C \ . \tag{3.43}$$

From the relation $J = 3K$ and the replacement of C with $3\,C = J(0) = 2H(0)$, equation (3.37) becomes

$$B(\tau_R) = \frac{\kappa_J(\tau_R)}{\kappa_P(\tau_R)}\left[3\int_0^{\tau_R} \frac{\kappa_F(\tau')}{\kappa_R(\tau')} H(\tau')\ d\tau' + 2\,H(0)\right] - \frac{\kappa_R(\tau_R)}{\kappa_P(\tau_R)}\frac{dH(\tau_R)}{d\tau_R} \ . \tag{3.44}$$

Following the same scheme presented in the previous subsection, the equation for the temperature correction can be obtained from equation (3.44),

$$\Delta T(\tau_R) = \frac{1}{16\,\sigma_R\,T(\tau_R)^3}\left\{\frac{\kappa_J(\tau_R)}{\kappa_P(\tau_R)}\left[3\int_0^{\tau_R} \frac{\kappa_F(\tau')}{\kappa_R(\tau')}\Delta F(\tau')\ d\tau' + 2\Delta F(0)\right] - \frac{\kappa_R(\tau_R)}{\kappa_P(\tau_R)}\frac{d\Delta F(\tau)}{d\tau_R}\right\} \ . \tag{3.45}$$

3.4 Theoretical model for the atmosphere

The following model is valid when the magnetic effects can be neglected, which occurs at $B \lesssim 10^9 \left(T/10^6\,\mathrm{K}\right)$ G as calculated in chapter 1. The independent variable is the Rosseland optical depth, τ_R. Calculations of the atmospheric model can be divided into two parts. In the first one the structure of the atmosphere is calculated solving the equation of hydrostatic equilibrium with respect to τ_R. In the second one the transfer equation is solved. The calculation starts from the temperature profile of a grey atmosphere (equation 3.25) which is corrected through the Lucy-Unsöld procedure. The compositions used are pure hydrogen, pure helium, pure carbon, pure oxygen and pure iron. The expression for the opacity has been chosen depending on whether the atmospheric medium is completely ionized or not. In order to disentangle between these two different cases, it is necessary to compare typical particle energy (which coincides with the thermal energy) $k_B\,T_{eff}$ with the total binding energy $E_b = Z^2\,13.6\,\mathrm{eV}$ (see Zavlin et al., 1996). If one considers hydrogen, then $k_B T_{eff} \gg 13.6\,\mathrm{eV}$ for all the effective temperatures considered in this thesis ($\log T_{eff}\,[\mathrm{K}] = 5.5 \div 6.25$). If the atmosphere is composed by helium, then it is completely ionized only for effective temperatures higher than $\log T_{eff}\,[\mathrm{K}] = 5.75$. In the cases of pure carbon, pure oxygen and pure iron the atmosphere can not be considered completely ionized. For a completely ionized atmosphere, the interactions between photon and matter are governed by the free-free process, for which the monochromatic free-free opacity is (see Rybicki & Lightman, 2008, for further details)

$$\kappa_\nu^{ff} = 3 \times 10^8 T^{-1/2} Z^2 \frac{n_e n_i}{\rho} \nu^{-3} \left(1 - e^{-h\nu/k_B T}\right) \bar{g}_{ff} \ \ \mathrm{cm^2\,g^{-1}} \tag{3.46}$$

and the Rosseland opacity is

$$\kappa_R^{ff} = 1.7 \times 10^{-25}\, T^{-7/2}\, Z^2 \frac{n_e n_i}{\rho} \bar{g}_R \ \ \mathrm{cm^2\,g^{-1}}\ , \tag{3.47}$$

where Z is the atomic number, n_e is the electron density, n_i is the ionic density, ρ is the mass density of the atmosphere, $\bar{g}_{ff}$ and $\bar{g}_R$ are the *Gaunt factors*. Also scattering effects need to be taken into account. The electron scattering opacity is $\kappa_s = \sigma_T\, n_e/\rho \sim 0.1\ \mathrm{cm^2 g^{-1}}$ where σ_T is the Thomson cross section. At energies close to the maximum of the blackbody, the

absorptive opacity is $\sim 10^3 - 10^5\ \mathrm{cm^2\,g^{-1}}$, so that scattering is negligible and scattering effects in the monochromatic opacity can be treated as a perturbation approximated as (see Romani, 1987)

$$\kappa_\nu = \kappa_\nu^{ff} + \left(\frac{\kappa_\nu^{ff}}{\kappa_\nu^{ff} + \kappa_s} \right)^{1/2} \kappa_s \,, \tag{3.48}$$

where the term $(\kappa_\nu^{ff}/(\kappa_\nu^{ff} + \kappa_s))^{1/2}$ corresponds to the number of scatterings before the photon is absorbed (see Rybicki & Lightman, 2008). For a partially ionized atmosphere it is necessary to take into account bound-bound and bound-free processes. The OP project takes these effects into account for the opacity computation (see Seaton et al., 1994).

Atmospheric structure

The equation of state used in this work is that for a perfect gas, $P = (n_e + n_i)\, k_B T$, where P is the pressure. For a typical NS atmosphere, the density is at most of the order of $10\ \mathrm{g\,cm^{-3}}$ (see Zavlin et al., 1996) which implies that the considered gas is non degenerate. For the energies considered (up to 10 keV), the gas is non relativistic, $\rho = m_e n_e + m_i n_i \simeq m_i n_i$: in fact the electron rest energy is 511 keV, which is much bigger than the thermal energy $k_B T$. The structure of the atmosphere is obtained by integrating the hydrostatic equilibrium equation

$$\frac{dP\left(\tau_R\right)}{d\tau_R} = \frac{g}{k_R\left(T\left(\tau_R\right), \rho\left(\tau_R\right)\right)} \tag{3.49}$$

starting from the surface, where $P\left(\tau_R = 0\right) = 0$. In the case of a completely ionized atmosphere it is possible to solve equation (3.49) analytically when the temperature profile corresponds to the grey temperature. Using the expression of density, the perfect gas relation and $n_e = Z\, n_i$ the expression for the Rosseland opacity can be re-written as

$$\kappa_R\left(\tau_R\right) = 1.7 \times 10^{-25} \frac{Z^3\, P\left(\tau_R\right)}{A\, m_p\, k_B\, T\left(\tau_R\right)^{9/2} \left(Z+1\right)} \bar{g}_R \,. \tag{3.50}$$

Using equation (3.49) and (3.25), equation (3.49) becomes

$$\frac{dP}{d\tau_R} = \frac{g\,A\,m_p\,k_B\,T_{eff}^{9/2}\,(Z+1)}{2.3\times10^{-25}\,Z^3\,\bar{g}_R}\,\frac{\left(\tau_R+\frac{2}{3}\right)^{9/8}}{P\,(\tau_R)}\,. \tag{3.51}$$

Equation (3.51) can be solved for separation of variables, giving

$$P\,(\tau_R) = \sqrt{\frac{g\,A\,m_p\,k_B\,T_{eff}^{9/2}\,(Z+1)}{2.5\times10^{-25}\,Z^3\,\bar{g}_R}\left[\left(\tau_R+\frac{2}{3}\right)^{17/8}-\left(\frac{2}{3}\right)^{17/8}\right]}\,. \tag{3.52}$$

If the atmosphere is not completely ionized or if the temperature profile does not follow the grey temperature then equation (3.49) has to be solved using a numerical method. Once determined the pressure with respect to τ_R then $n_e\,(\tau_R)$ and $n_i\,(\tau_R)$ are known.

Radiation transfer

The emergent spectra are computed using the Schwarzschild-Milne equation

$$F_\nu\,(\tau_\nu) = 2\pi\left[\int_{\tau_\nu}^{\infty} dt\,S_\nu\,(t)\,E_2\,(t-\tau_\nu) - \int_0^{\tau_\nu} dt\,S_\nu\,(t)\;E_2\,(\tau_\nu - t)\right]\,, \tag{3.53}$$

where, due to the assumption of LTE (*assumption 4*), $S_\nu\,(t) = B_\nu\,(T\,(\tau_R\,(t)))$. The monochromatic optical depth is computed as a function of the Rosseland optical depth τ_R solving the differential equation

$$\frac{d\tau_\nu}{d\tau_R} = \frac{k_\nu\,(\tau_R)}{k_R\,(\tau_R)}\,, \tag{3.54}$$

which has been obtained by the ratio between $d\tau_\nu = -\rho k_\nu dz$ and $d\tau_R = -\rho k_R dz$. The integration of equation (3.53) over the frequencies gives the total flux $F\,(\tau_R)$ which in radiative equilibrium should be constant at $F_{eff} = \sigma_{SB}T_{eff}^4$. The departures from constancy $\Delta F = F_{eff} - F\,(\tau_R)$ are used to estimate the correction to the temperature using the Lucy-Unsöld procedure (equation 3.45).
The new temperature is used to re-compute the atmospheric structure, the flux and the corrections. This procedure is iterated until the radiative equilibrium is reached.

3.5 The effects of magnetic field

For the sake of completeness, here the effects of magnetic effects are taken into account. However, in the next chapter only the model implementation in the presence of weak magnetic fields will be discussed. The substantial difference with respect to the non-magnetic atmosphere model is the fact that the magnetic field makes the medium anisotropic. This implies that the radiative transfer should be solved through two equations, for the ordinary and the extraordinary photons. The total flux, which in radiative equilibrium has to be equal to $\sigma_{SB}\, T_{eff}^4$, is obtained by the integration of equation (2.51)

$$F \simeq -c \int d\nu \left(l_1 \frac{\partial u_\nu^1}{\partial \tau} + l_2 \frac{\partial u_\nu^2}{\partial \tau} \right) n_e \sigma_T = \sigma_{SB} T_{eff}^4 \,. \tag{3.55}$$

As in non-magnetic case, the theoretical model can be divided into two parts: (i) solution of the atmospheric structure; (ii) solution of the transfer equations. In this case the independent variable is the Thomson optical depth τ.
The structure of the atmosphere and therefore the numerical densities can be computed by merging the equation of state of an ideal gas, $P = (n_e + n_i) k_B T$, and the hydrostatic equilibrium condition:

$$\frac{dP}{dz} = \rho g \quad \Longrightarrow \quad \frac{dP}{d\tau} = \frac{m_p\, g}{\sigma_T} \,, \tag{3.56}$$

whose solution is $P = m_p\, g\, \tau / \sigma_T$.
To solve the radiative transfer, the following equation is used

$$\frac{\partial}{\partial \tau} \left(\frac{l_j}{l_0} \frac{\partial u_\nu^j}{\partial \tau} \right) = \frac{K_j^{abs}}{\kappa^s} \left(u_\nu^j - \frac{u_\nu^P}{2} \right) + \frac{K_{21}^s}{\kappa^s} \left(u_\nu^j - u_\nu^{3-j} \right) \tag{3.57}$$

and it is derived in section 2.4. The monochromatic flux is computed through the formula

$$F_{\nu,z}^j \sim -c\, l_j \frac{\partial u_\nu^j}{\partial z} \,. \tag{3.58}$$

which integrated over frequencies gives the total flux. The procedure to solve the transfer equation is iterative. Starting from the approximation of grey temperature (equation (3.25)), the correction temperature can be obtained

through the equation (see Shibanov et al., 1992)

$$\Delta T = -\frac{f}{df/dT};\ f = \int d\nu \sum_j \kappa_j \left(J_j - \frac{1}{2} B_\nu \right) . \tag{3.59}$$

The iterative process terminates when radiative equilibrium is reached.

Chapter 4

Numerical simulations

In the following chapter the numerical implementation of the atmosphere model described in section 4.4 is discussed. In the first section the implementation of the code is exposed, while the simulation results are discussed in the following ones.

4.1 The code

In order to simulate the properties of radiation emitted from a NS and reprocessed in its atmospheric layer, a Fortran 95 code has been developed. To obtain the emergent flux it is necessary to compute the opacities which are related to the quantities of the atmosphere medium, i.e. its electron numerical density and temperature. The expressions of the opacities depend on the complete or partial ionization of the atmosphere, discussed in details in section 3.4. In the fully ionized case the opacity is given by

$$\kappa_\nu = \kappa_\nu^{ff} + \left(\frac{\kappa_\nu^{ff}}{\kappa_\nu^{ff} + \kappa_s} \right)^{1/2} \kappa_s \,, \tag{4.1}$$

while in the other case the opacity is taken from the OP project. As it will be explained in the following, the second case sets numerical boundaries on the independent variables, which are the Rosseland optical depth and the photon energy. For this reason, in the following, the treatment and the code is divided in full and partial ionized atmosphere.

4.1.1 Fully ionized atmosphere

The independent variables considered in the code are:

- the Rosseland optical depth τ_R, defined over a discrete grid composed by $N_\tau = 100$ logarithmically spaced points between 10^{-3} and 500;

- the photon energy (written in units of $k_B T_{eff}$), defined over a discrete grid composed by $N_E = 80$ logarithmically spaced points between 0.1 and 50.

The structure of the atmosphere is solved by imposing the hydrostatic equilibrium condition:

$$\frac{dP}{d\tau_R} = \frac{g}{\kappa_R(\tau_R)}\,. \tag{4.2}$$

The numerical simulation starts from an approximate grey atmosphere with a temperature profile $T(\tau_R) = T_{eff}\left[3/4\,(\tau_R + 2/3)\right]^{1/4}$ and equation (4.2) is analytically solved (the solution is reported in equation 3.52). When the correction of the temperature is applied, the numerical solution is performed using a Runge-Kutta-Merson method, which requires as input the initial condition $(\tau_{R_1}, P(\tau_{R_1}))$, where $\tau_{R_1} = 0.001$ is the first value of the grid, and the relative accuracy (set to 10^{-3}); the output of the routine is the value of the pressure at the desired τ_R. A reasonable initial condition, $P(\tau_{R_1})$ is the value of the pressure computed in the grey approximation.
To solve the radiative transfer, it is necessary to compute the value of the monochromatic optical depth τ_ν as a function of τ_R, through the solution of equation

$$\frac{d\tau_\nu(\tau_R)}{d\tau_R} = \frac{\kappa_\nu(\tau_R)}{\kappa_R(\tau_R)}\,. \tag{4.3}$$

Also this equation is numerically solved through the Runge-Kutta-Merson routine with initial condition $\tau_\nu(\tau_{R_1}) = 0$ for each value of energy and the relative accuracy is chosen as 0.001. Once determined the monochromatic optical depth, it is possible to solve the expression for the energy flux:

$$F_\nu(\tau_\nu) = 2\pi\left[\int_{\tau_\nu}^{\infty} dt\, B_\nu\left(T(\tau_R(t))\right) E_2(t-\tau_\nu) - \int_0^{\tau_\nu} dt\, B_\nu\left(T(\tau_R(t))\right)\, E_2(\tau_\nu - t)\right]\,. \tag{4.4}$$

The integrals of equation (4.4) are numerically solved through the Romberg integration method, which requires as input the integrating function and the upper and lower bounds. The upper bound of the first integral is set to $\tau_\nu + 20$ because the contributions to the integral for values of $|t - \tau_\nu| \geq 20$ are negligible. For the same reason the lower bound of the second integral is chosen as the maximum value between $\tau_\nu - 20$ and 0. The computation of the total flux $F(\tau_R) = \int d\nu F_\nu(\tau_\nu)$ is performed through the Piecewise Cubic Hermite Interpolant Package (PCHIP, see Fritsch, 2015, and reference therein) which allows the integral calculation with discrete values. Then, the temperature correction procedure can be computed through the total flux expression

$$\Delta T(\tau_{R_i}) = \frac{1}{16\,\sigma_R\,T(\tau_{R_i})^3}\left\{3\int_{\tau_{R_1}}^{\tau_{R_i}}\frac{\kappa_F(\tau')}{\kappa_R(\tau')}\Delta F(\tau')\,d\tau' + 2\Delta F(\tau_{R_1}) - \frac{\kappa_R(\tau_{R_i})}{\kappa_P(\tau_{R_i})}\frac{d\Delta F(\tau_{R_i})}{d\tau_{R_i}}\right\}, \tag{4.5}$$

where the Planck and flux opacities are defined respectively in equation (3.39) and (3.42). The quantities κ_P, κ_F and the integral in equation (4.5) are computed exploiting the PCHIP code. The corrected temperature allows to iterate the procedure to solve the atmospheric structure and to re-compute the fluxes until radiative equilibrium is reached. In numerical simulations the convergence occurs when the relative maximum error, $\max[\Delta F(\tau_{R_i})]/F_{eff}$, is $\sim 1\%$. Figure 4.1 shows the convergence of the iterative procedure with respect to the number of iteration in the case of a hydrogen atmosphere at $\log T_{eff}\,[K] = 6$. The first iteration (red line) has a relative average error, $\sum \Delta F(\tau_{R_i})/N_\tau F_{eff}$, of $\sim 20\%$ with a maximum of 30%. The last iteration (light-blue line), when radiative equilibrium is reached, has an average error $\lesssim 5‰$ with a maximum error $\sim 1\%$.

4.1.2 Partially ionized atmosphere

In this case, the monochromatic opacities are taken from the OP project, as consequence, the independent variables are subjected to numerical boundaries. These monochromatic opacities rely on different energy ranges at different temperatures T and electronic numerical densities n_e. This implies that at a fixed energy it is not guaranteed the existence of the corresponding

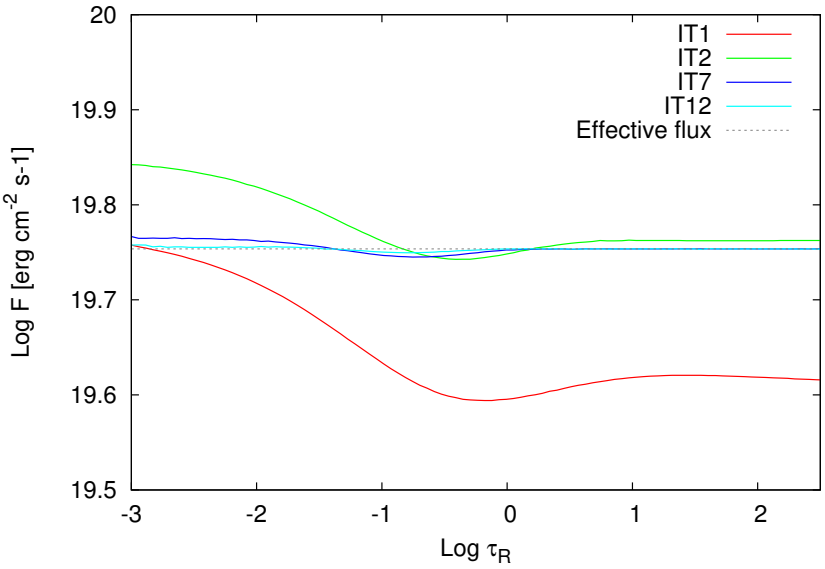

Figure 4.1: Total flux as a function of the optical depth for different iterations. This plot shows the convergence of the iterative procedure with respect to the number of iterations. The first iteration (red line) has a relative average error $\sim 20\%$ with a maximum of 30% while the second iteration (green line) has an average error $\sim 7\%$ with a maximum of $\sim 20\%$. The seventh iteration (blue line) is affected by a definitive lower error: its maximum error is $\sim 3\%$. The last iteration (light blue line), at which convergence is reached, has an average error $\lesssim 5‰$ and a maximum error which is lower than 1%.

opacity κ_ν for all combinations of T and n_e (i.e. for all τ_R); therefore, from the relation (4.3), neither τ_ν can be computed for all the values of τ_R and vice versa. The above consideration introduces problems in the numerical integration of equation (4.4) where τ_ν is the integration variable on which $\tau_R(\tau_\nu)$ depends. If the energy range is such that τ_ν exists for all energies and for all τ_{R_i}, the numerical integration can be computed without any type of complication.
To find the energy range which satisfies this constraint it is necessary to proceed in the following way. The energy range over which the OP project monochromatic opacities exist spans from 0.1 and 20 in units of $k_B T(\tau_R)$. As a consequence the energy range is monotonically increasing with τ_R, being temperature monotonically increasing with respect to τ_R. The desired energy range is then obtained by considering the intersection between the energy ranges associated to the minimum and the maximum value of the Rosseland optical depth grid. The resulting energy range is sampled in 80 energy points logarithmically spaced. The Rosseland optical depth is defined over a discrete grid composed by 100 points, also logarithmically spaced, between 10^{-3} and 50.
In order to solve equation (4.2) the initial value of the pressure $P(\tau_{R_1})$ needs to be computed in a different way with respect to the fully ionized case. Since the interval $0 - \tau_{R_1}$ is small, the derivative of the pressure, given by equation (4.2), is considered as constant (see Gänsicke et al., 2002). In this way the initial condition is $P\left(\tau_{R_1} = 10^{-3}\right) = g/\kappa_R(\tau_{R_1})\,\tau_{R_1}$. The other numerical computations are the same of the fully ionized case.

4.2 Simulation results

In the following the results of the atmosphere model for hydrogen, helium, carbon, oxygen and iron compositions are presented and discussed. The model is applied at different effective temperatures, $\log T_{eff}\,[\mathrm{K}] = 5.5$, 5.75, 6 and 6.25 for a surface gravity $g_{14} = g/(10^{14}\,\mathrm{cm\,s^{-}}2) = 2.43$ (see Zavlin et al., 1996). Then, the comparisons between different chemical compositions and different surface gravities are shown. The aim is to highlight how the chemical composition and the surface gravity influence the behaviour of the NS emergent spectrum.

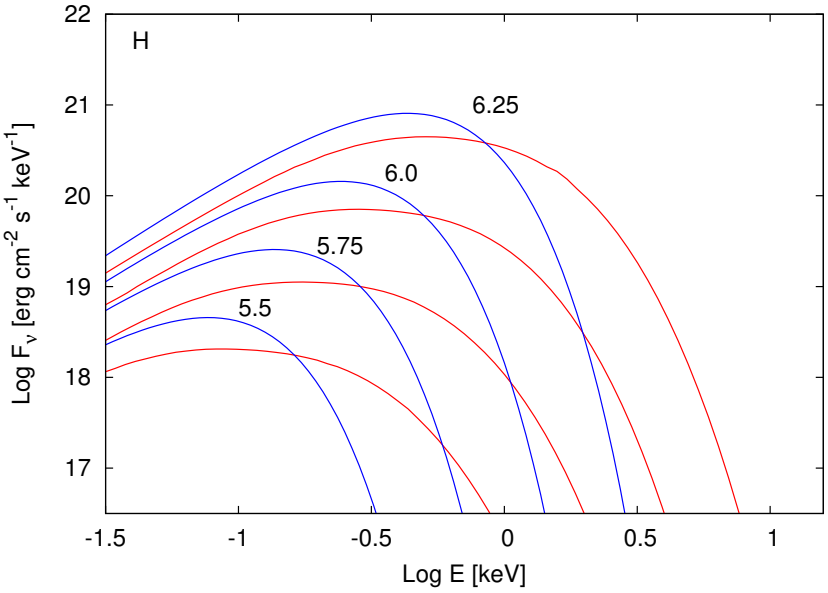

Figure 4.2: Emergent spectra for a hydrogen atmosphere at different effective temperatures (numbers labelling the curves give $\log T_{eff}$ [K]). The blackbody spectra are also shown for comparison (blue lines).

4.2.1 Hydrogen atmosphere

As already mentioned, a hydrogen NS atmosphere is completely ionized at all the effective temperatures considered. Figure 4.2 shows the emergent spectra at different effective temperatures. It can be noted that the spectra differ substantially from the blackbody spectrum (blue line) at the corresponding temperature, especially at high energies where the simulated spectra are harder than the corresponding blackbody spectra. At low energies the flux have the same slope of the blackbody (Rayleigh-Jeans tail) but with lower values. The monochromatic opacity, shown in Figure 4.3, has a decreasing behaviour with the photon energy, with a difference of ~ 6 orders of magnitude between the values assumed at low energies (0.01 keV) and at high energies (1 keV). This is essentially explained by the fact that free-free opacity follows the Kramers' law, $k_\nu \sim \nu^{-3}$. According to the behaviour reported in Figure 4.3 one can expect that high-energy photons will escape the atmosphere more easily than low-energy ones, which instead remain trapped.

4.2.2 Helium atmosphere

In Figure 4.4 the simulated spectra of a helium atmosphere at different effective temperatures are shown, compared with the corresponding blackbody distributions. As in the case of the hydrogen atmosphere, a hard excess appears with respect to the blackbody at high photon energies and the spectra follow the Rayleigh-Jeans behaviour at low energies. Similarly, the behaviour of the spectra can be explained observing the monochromatic opacities, which are shown in Figure 4.6 (right panel). The spectra in Figure 4.4 are simulated in the complete ionization hyphothesis at all the effective temperatures, although it is not correct for temperatures lower than $\log T_{eff}\,[\mathrm{K}] = 6$. Figure 4.5 shows a comparison between the simulated spectra with a complete ionization (green lines) and a partial ionization (red lines) at effective temperatures $\log T_{eff}\,[\mathrm{K}] = 5.5$ and 5.75. The main difference between the two cases is the absorption feature that occurs in the partial ionized atmosphere at around 30 eV. In particular for $\log T_{eff}\,[\mathrm{K}] = 5.5$, the latter can be understood looking at the opacity represented in Figure 4.6 (left panel). At around 30 eV the opacity suddenly increases and therefore a greater number of photons at those energies remain trapped in the atmosphere.

At large optical depths, the Rosseland approximation

$$F_\nu(z) = -\frac{4\pi}{3}\,\frac{1}{\alpha_\nu}\,\frac{\partial B_\nu}{\partial T}\,\frac{d\,T}{d\,z} \tag{4.6}$$

is valid. Figure 4.7 shows how well the numerical simulation reproduces the theoretical prediction for a hydrogen atmosphere (left panel) and for a helium atmosphere (right panel) at $\log T_{eff}\,[\mathrm{K}] = 6$.

4.2.3 Carbon, oxygen and iron atmosphere

For carbon, oxygen and iron compositions the atmosphere can not be treated as completely ionized at the effective temperatures considered. In Figure 4.8 the simulated emergent spectra for a carbon atmosphere are shown. The way in which the spectrum changes is different at different effective temperatures. This is due to the fact that the monochromatic opacity has a different profile at different temperatures as shown in Figure 4.9. The flux behaviour can be explained observing the corresponding opacity, e.g.

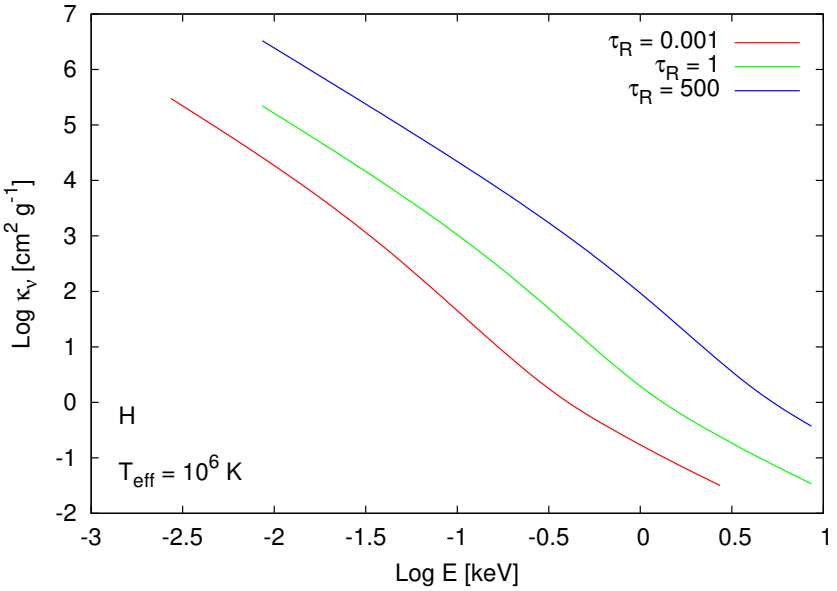

Figure 4.3: Monochromatic opacity plotted as a function of the photon energy at different Rosseland optical depths for a hydrogen atmosphere.

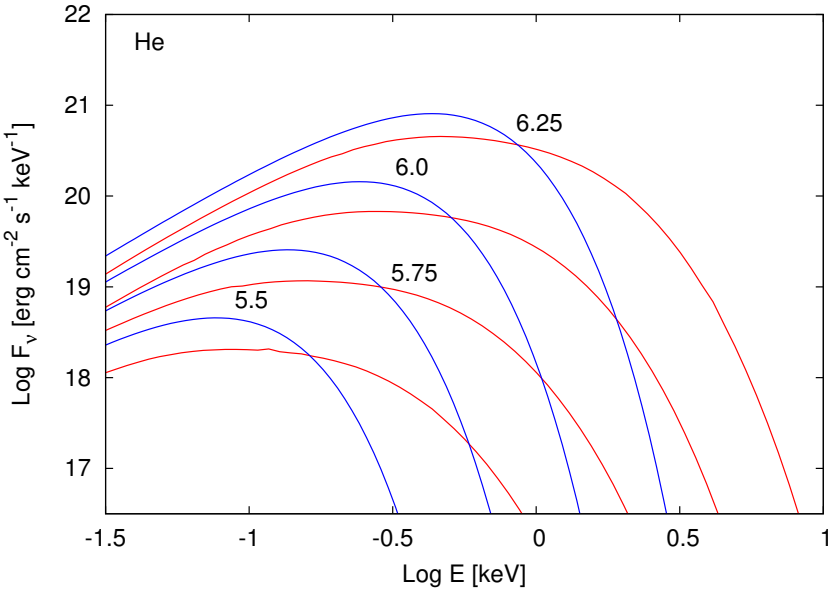

Figure 4.4: Same as in Fig. 4.2 for a completely ionized He atmosphere.

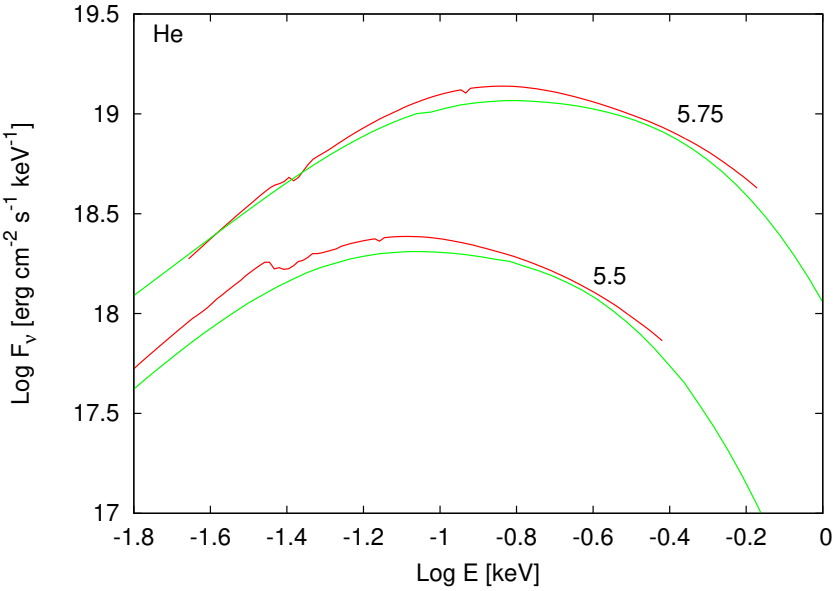

Figure 4.5: Emergent spectra of a helium atmosphere at $\log T_{eff}[\mathrm{K}] = 5.5, 5.75$. The red lines refer to models computed with the OP opacity and the green ones to those computed with the free-free opacity.

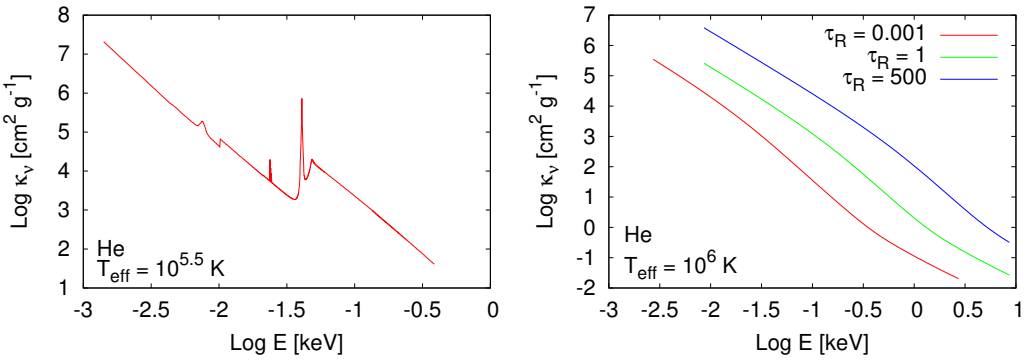

Figure 4.6: Monochromatic opacity plotted as a function of the photon energy for helium. The left panel shows the OP monochromatic opacity at $\log T_{eff}[\mathrm{K}] = 5.5$ for which the helium is partially ionized while the right panel shows the monochromatic opacity at $\log T_{eff}[\mathrm{K}] = 6$ when helium is completely ionized.

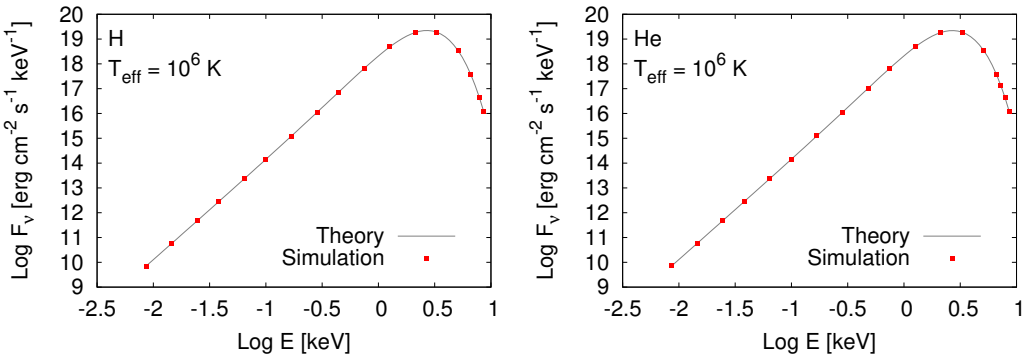

Figure 4.7: Monochromatic flux plotted as a function of the photon energy at high τ_R. In the left panel the atmospheres is composed by hydrogen while in the right panel by helium. In both cases the effective temperature is 10^6 K.

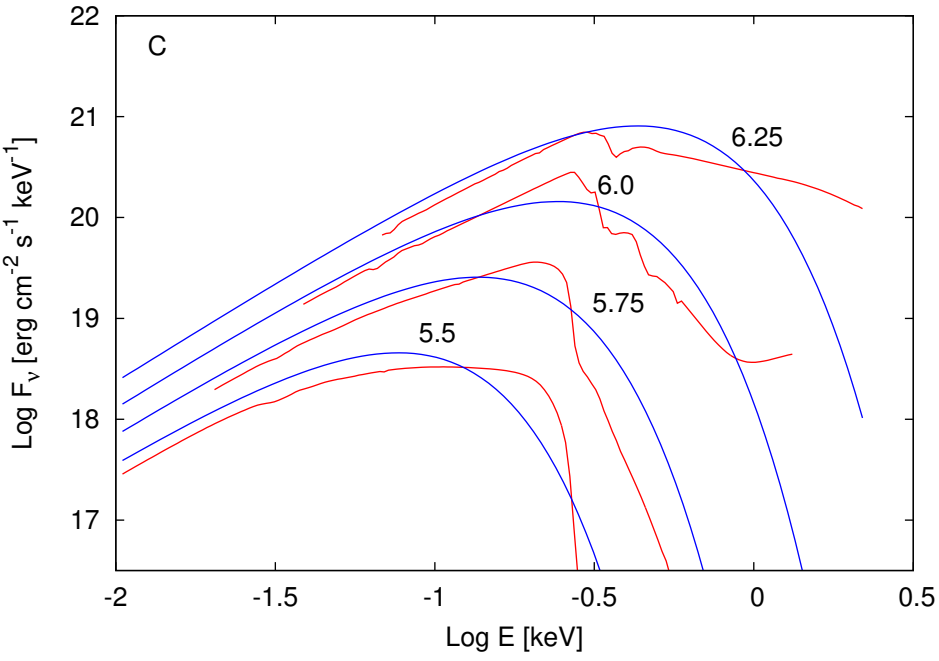

Figure 4.8: Same as in Fig. 4.2 for a carbon atmosphere.

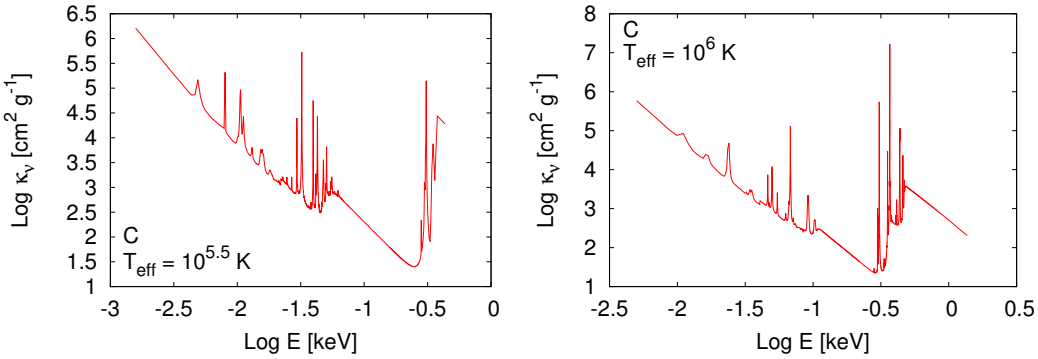

Figure 4.9: Monochromatic opacity plotted as a function of the photon energy for carbon. The left panel shows the opacity at $\log T_{eff}[\mathrm{K}] = 5.5$ and the right panel at $\log T_{eff}[\mathrm{K}] = 6$.

the simulated emergent spectrum at $\log T_{eff}[\mathrm{K}] = 5.5$ shows an excess with respect to the blackbody in the energy range of $\log E[\mathrm{keV}]$ between -0.8 and -0.6 while at $\log E[\mathrm{keV}] \sim -0.5$ the flux suddenly falls down. Observing the left panel of Figure 4.9 in the energy range $\log E[\mathrm{keV}]$ between -0.8 and -0.6 the monochromatic opacity decreases, thus a larger number of photons can escape. At energies $\log E[\mathrm{keV}] \sim -0.5$ the opacity rapidly increases, therefore a lower number of photons can emerge. The same argument can be applied for the flux at $\log T_{eff}[\mathrm{K}] = 6$ observing the corresponding opacity (right panel of Figure 4.9).

In Figure 4.10 the simulated emergent spectra for an oxygen atmosphere, compared with the corresponding blackbody distributions, are shown. As in the case of the carbon atmosphere, the behaviour of the flux can be understood observing the corresponding opacities which are shown in Figure 4.11 at effective temperatures $\log T_{eff}\,[\mathrm{K}] = 5.5$ and 6.

Figure 4.12 shows the simulated flux for an iron atmosphere. Except for the flux at $\log T_{eff}[\mathrm{K}] = 5.5$, the other fluxes of oxygen and iron atmospheres follow closer the blackbody spectra.

Figure 4.13 shows the monochromatic opacity for iron taken from the OP project file (left panel) and the monochromatic opacity used in the code (right panel). For heavy elements one can expect that there are a lot of absorption features. However this behaviour is not found in the simulated spectra because the opacities used in the code are binned in 200 energy points while they are binned in 10^4 points in the OP project files, showing

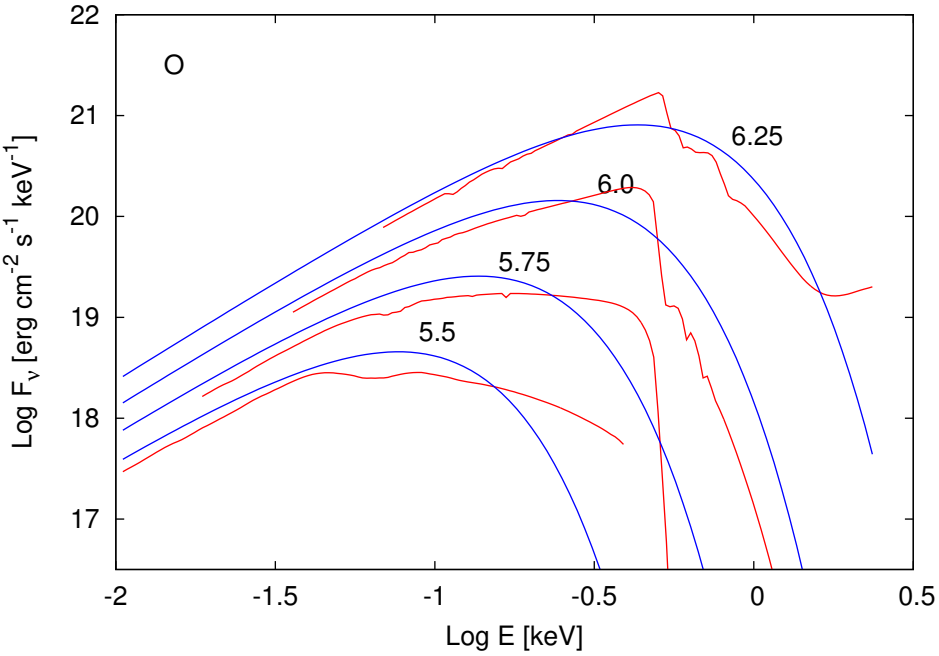

Figure 4.10: Same as in Fig. 4.2 for an oxygen atmosphere.

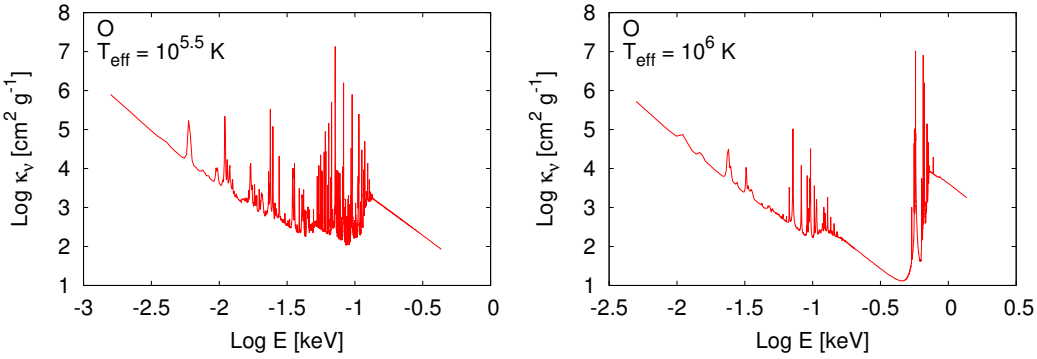

Figure 4.11: Monochromatic opacity plotted as a function of photon energy for oxygen. The left panel shows the opacity at $\log T_{eff}[\mathrm{K}] = 5.5$ and the right panel at $\log T_{eff}[\mathrm{K}] = 6$.

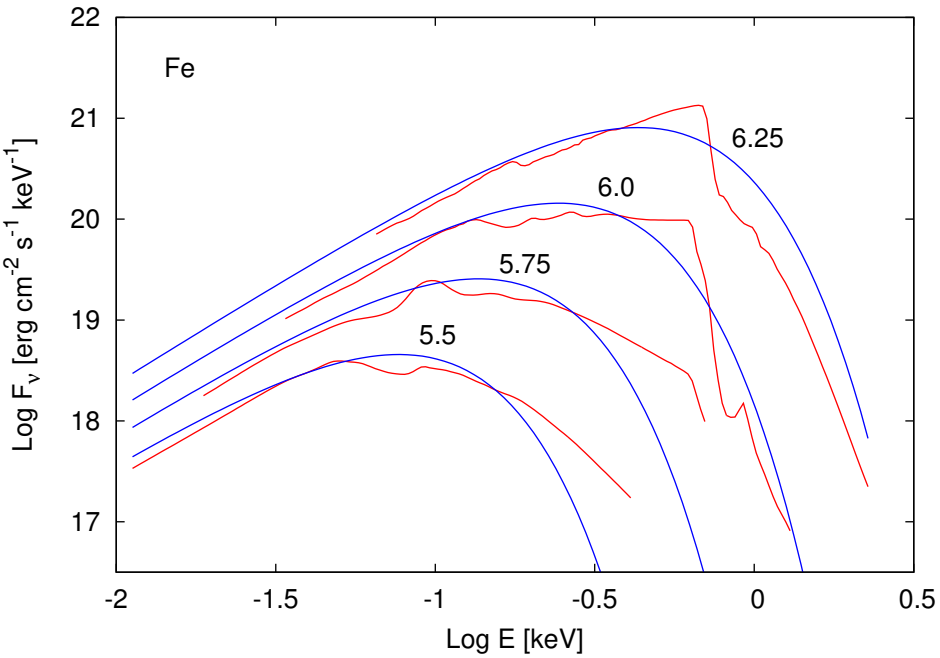

Figure 4.12: Same as in Fig. 4.2 for an iron atmosphere.

more spectral features.

Figure 4.14 shows the emergent spectra for different chemical compositions at two effective temperatures $\log T_{eff}[\mathrm{K}] = 5.5$ (left panel) and 6 (right panel). It can be noticed that the behaviour of the emergent spectra depend strongly on chemical composition. The chemical composition affects the monochromatic opacity. For light elements, where the atmosphere can be considered completely ionized, the monochromatic free-free opacity follows the Kramers' law ($\kappa_\nu \sim \nu^{-3}$) at high energies which implies that a great number of photons can emerge. For heavy elements, to compute the monochromatic opacity, one needs to take into account, not only the free-free term, but also the bound-free and the bound-bound terms (see Figure 4.9 and 4.13). This causes the opacity to have a more irregular shape but, on average, it is flatter than the free-free one, which in turns means that the spectrum follows a blackbody more closely (see Zavlin et al., 1996).

Figure 4.15 shows the simulated spectra for hydrogen (left panel) and iron (right panel) at effective temperature $\log T_{eff}\,[\mathrm{K}] = 6$, at different surface gravities $g_{14} = 1.18$ (red line), 1.59 (green line) and 2.43 (blue line). The spectra are almost the same, therefore the atmosphere model developed

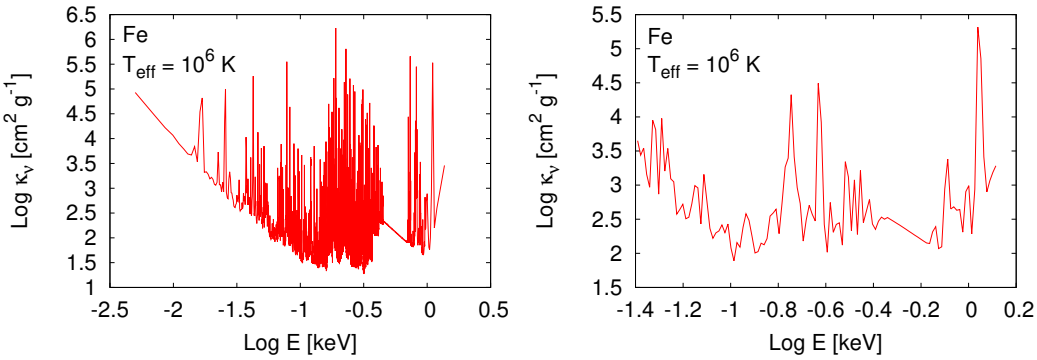

Figure 4.13: Monochromatic opacity plotted as a function of photon energy for an iron atmosphere at $\log T_{eff}[\mathrm{K}] = 6$. The left panel shows the monochromatic opacity with 10^4 energy points while the right panel shows the monochromatic opacity with 200 points, used by the code.

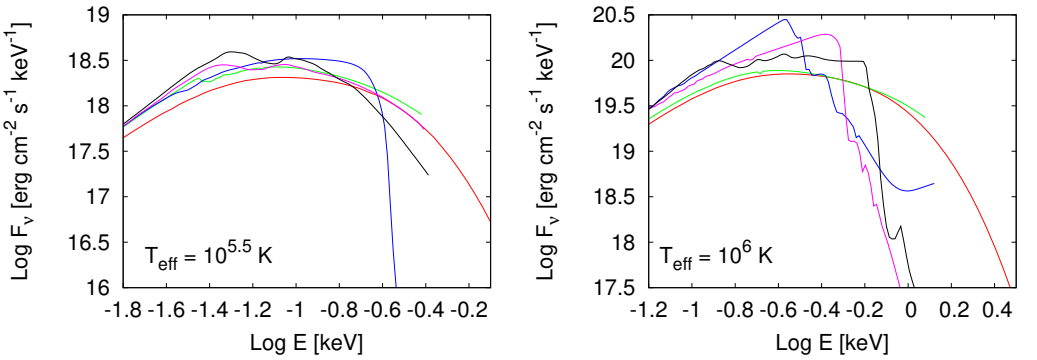

Figure 4.14: Emergent spectra for different chemical compositions. The left panel shows the spectra computed at $\log T_{eff}[\mathrm{K}] = 5.5$ while the right panel at $\log T_{eff}[\mathrm{K}] = 6$. The red lines correspond to an hydrogen atmosphere, the green lines to a helium atmosphere, the blue lines to a carbon atmosphere, the purple lines to an oxygen atmosphere and the black lines to an iron atmosphere.

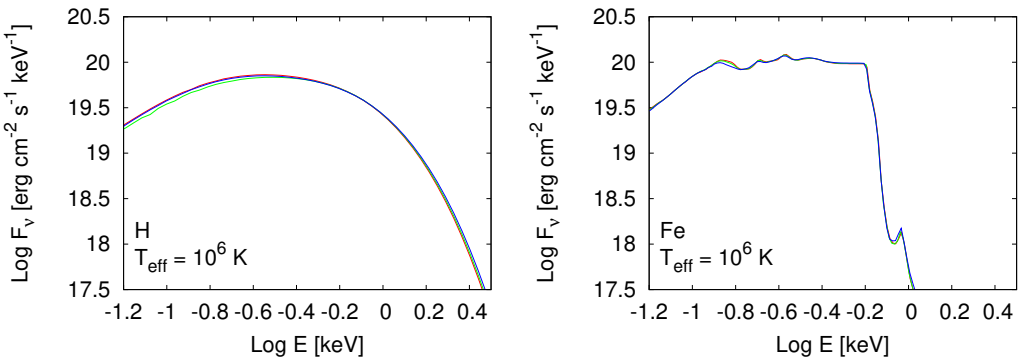

Figure 4.15: Simulated spectra for hydrogen (left panel) and iron (right panel) atmospheres for different values of the surface gravity: $g_{14} = 1.18$ (red lines), 1.59 (green lines) and 2.53 (blue lines). The effective temperature is set at 10^6 K.

seems to be independent from the surface gravity.

Chapter 5

Conclusions

In this thesis the re-procession of NS surface radiation by a thin atmospheric layer is studied. From the analysis of the spectra, it is possible to infer some NS parameters, e.g. the effective temperature, the chemical composition of the atmosphere and the surface gravity, therefore the ratio between mass and radius.
The performed numerical simulations are based on a NS with low magnetic field, $B \lesssim 10^9$ G, for which magnetic effects can be neglected.
The method used to solve the radiative transfer is based on an iterative scheme starting from an approximated temperature profile. The procedure is divided into two parts: in the first one the calculation of the atmospheric structure is performed while in the second one the radiative transfer is computed using the Schwarzschild-Milne relation. To complete an iteration, a correction of the temperature through the Lucy-Unsöld formula is applied; a new iteration starts computing the structure and the flux again, until the radiative equilibrium is reached. In the code considered, this condition occurs when the relative maximum error, $\max\left[\Delta F\left(\tau_{R_i}\right)\right]/F_{eff}$, is $\sim 1\%$. Figure 4.1 shows the convergence of the iterative procedure. At large Rosseland optical depths, where Rosseland approximation holds, it is possible to test the accordance between numerical simulation and the theoretical prediction as shown in Figure 4.7.
Different ranges for the effective temperature ($\log T_{eff}\,[\mathrm{K}] = 5.5,\ 5.75,\ 6,\ 6.26$) and the surface gravity ($g_{14} = 1.18,\ 1.59,\ 2.43$) have been explored, while the atmosphere compositions considered have been hydrogen, helium, carbon, oxygen and iron.

It is possible to compare how the emergent spectrum changes when one of the three parameters is not fixed.
Taking the surface gravity and the chemical composition fixed but varying the effective temperature, one notes that, for light elements, e.g. hydrogen and helium, the emergent spectrum does not change in its trend but only in intensity. Comparing the simulated spectra with correspondent blackbody distributions, it is possible to observe a hard excess at high photon energies as shown in Figures 4.2 and 4.4. For heavier elements the form of the spectrum depends hardly on the effective temperature; in these cases the simulated spectra follow closer the blackbody distributions with the presence of spectral features as shown in Figures 4.8, 4.10 and 4.12.
At different surface gravities the spectra remains almost the same, this shows the independence of the model on the surface gravity values.
For different chemical compositions but at fixed g and T_{eff} the spectra change considerably, because of the bound-free and the bound-bound interactions. The behaviour of the spectrum depends substantially on the opacity: for light elements, for which the atmosphere is fully ionized, the interactions are free-free and the opacity follows the Kramers' law ($\kappa_\nu \sim \nu^{-3}$), producing the excesses in the spectra at high energies; for heavier elements, the bound-free and the bound-bound interactions cause, as expected, the opacity to have a more irregular shape but, on average, it is flatter than the free-free one, which in turns means that the spectrum follows a blackbody more closely.
This thesis is far from being a complete and exhaustive work on the NS atmosphere. One of the possible improvements is to consider a more sophisticated equations of state, e.g. solving the equation of ionization equilibrium. Here the treatment about strongly magnetized atmospheres is discussed only from a theoretical point of view, but future works will include the numerical implementation.

Bibliography

Baade W., Zwicky F., 1934, PNAS, 20(5), 259

Burke-Spolaor S., 2013, Proceedings of the International Astronomical Union, 291, 95

De Luca A., 2008, AIP Conf. Proc., 983, 311

Fritsch F., 2015, `https://people.sc.fsu.edu/~jburkardt/f_src/pchip/pchip.html`

Gänsicke B. T., Braje T. M., Romani R. W, 2002, A&A, 386, 1001

Gnedin, I. N., Pavlov, G. G., 1974, Soviet Journal of Experimental and Theoretical Physics, 38, 903

Haensel P., Potekhin A., Yakovlev D.G., 2007, Neutron stars 1: Equation of state and structure, Springer Science & Business Media

Hewish A., Bell S.J., Pilkington J.D.H., Scott P.F., Collins R.A., 1968, Nature, 217, 709

Ho W., Lai D., 2001, MNRAS, 327, 1081

Huebner W. F., Mertz A. L., Magee N. H. Jr., Argo M. F. 1977, Astrophysical Opacity Library, Los Alamos Report LA-6760-M

Kaspi V., 2010, PNAS, 107, 7147

Iglesias C. A., Rogers F. J., Wilson B. G. 1992, ApJ, 397, 717

Lim Y., Hyun C. H., Lee C., 2017, International Journal of Modern Physics E, 26

Mészáros P., 1992, High-energy radiation from magnetized neutron stars, University of Chicago Press

Mihalas D., 1978, Stellar atmospheres

Rajagopal M., Romani R., 1996, ApJ, 461, 327

Rybicki G. B., Lightman A. P., 2008, Radiative processes in astrophysics, John Wiley & Sons.

Romani R., 1987, ApJ, 313, 718

Schwarzschild, K., 1914, Über Diffusion und Absorption in der Sonnenatmosphäre, Sitz. Ber. KgL Preuss. Akad. d. Wiss. Berlin.

Seaton M.J., Yu Yan, Mihalas D., Pradhan A.K., 1994, MNRAS 266, 805

Shapiro S.L., Teukolsky S. A., 1983, Black holes, White Dwarfs and Neutron Stars, Wiley

Shibanov I. A., Zavlin V. E., Pavlov G. G., Ventura J., 1992, AA, 266, 313

Turolla R., Zane S., Watts A. L., 2015, Reports on Progress in Physics 78.11

Zavlin V. E., Pavlov G. G., Shibanov, Yu. A., 1996, A&A, 315, 141